Pharm Res (2012) 29:1344–1365
DOI 10.1007/s11095-011-0661-9

RESEARCH PAPER

Silica-Iron Oxide Magnetic Nanoparticles Modified for Gene Delivery: A Search for Optimum and Quantitative Criteria

Olga Mykhaylyk • Titus Sobisch • Isabella Almstätter • Yolanda Sanchez-Antequera • Sabine Brandt • Martina Anton • Markus Döblinger • Dietmar Eberbeck • Marcus Settles • Rickmer Braren • Dietmar Lerche • Christian Plank

Received: 4 August 2011 / Accepted: 19 December 2011 / Published online: 6 January 2012

ABSTRACT

Purpose To optimize silica-iron oxide magnetic nanoparticles with surface phosphonate groups decorated with 25-kD branched polyethylenimine (PEI) for gene delivery.

Methods Surface composition, charge, colloidal stabilities, associations with adenovirus, magneto-tranduction efficiencies, cell internalizations, *in vitro* toxicities and MRI relaxivities were tested for the particles decorated with varying amounts of PEI.

Results Moderate PEI-decoration of MNPs results in charge reversal and destabilization. Analysis of space and time resolved concentration changes during centrifugation clearly revealed that at >5% PEI loading flocculation gradually decreases and sufficient stabilization is achieved at >10%. The association with adenovirus occurred efficiently at levels over 5% PEI, resulting in the complexes stable in 50% FCS at a PEI-to-iron *w/w* ratio of ≥7%; the maximum magneto-transduction efficiency was achieved at 9–12% PEI. Primary silica iron oxide nanoparticles and those with 11.5% PEI demonstrated excellent r_2* relaxivity values (>600 s^{-1}(mM Fe)$^{-1}$) for the free and cell-internalized particles.

Conclusions Surface decoration of the silica-iron oxide nanoparticles with a PEI-to-iron *w/w* ratio of 10-12% yields stable aqueous suspensions, allows for efficient viral gene delivery and labeled cell detection by MRI.

KEY WORDS colloidal stability · magnetic nanoparticles · MRI relaxivity · silica-polyethylenimine coating · transduction

ABBREVIATIONS

ATCC	American Type Culture Collection
DMEM	Dulbecco's modified Eagle's medium
EDTA	Ethylenediaminetetraacetic acid
FCS	fetal calf serum
ME-FFE	multi-echo gradient echo
MNP	magnetic nanoparticles
mPDAC	mouse pancreatic ductal adenocarcinoma
MRI	magnetic resonance imaging
PBS	Dulbecco's phosphate buffered saline
PEI	polyethylenimine
SIO-MNP	silica-iron oxide magnetic nanoparticle
SiO_x	silica-like coating of the iron oxide nanoparticles
TEM	Transmission Electron Microscopy
TEOS	tetraethyl orthosilicate
THPMP	3-(trihydroxysilyl) propylmethylphosphonate
TU	transducing units
VP	virus particle
XPS	X-ray photoelectron spectroscopy

Electronic supplementary material The online version of this article (doi:10.1007/s11095-011-0661-9) contains supplementary material, which is available to authorized users.

O. Mykhaylyk (✉) · Y. Sanchez-Antequera · S. Brandt · M. Anton · C. Plank
Institute of Experimental Oncology and Therapy Research
Klinikum rechts der Isar der Technischen Universität München
Ismaningerstrasse 22
81675 Munich, Germany
e-mail: olga.mykhaylyk@lrz.tu-muenchen.de

T. Sobisch · D. Lerche
LUM GmbH
Rudower Chaussee 29 (OWZ), 12489 Berlin, Germany

I. Almstätter · M. Settles · R. Braren
Department of Radiology, Klinikum rechts der Isar, Technische Universität München, Munich, Germany

M. Döblinger
Department of Chemistry, Ludwig-Maximilians-Universität München
Munich 81377, Germany

D. Eberbeck
Physikalisch-Technische Bundesanstalt
Abbestraße 2-12, 10587 Berlin, Germany

INTRODUCTION

Since the first publications on magnetically enhanced nucleic acid delivery, also known as magnetofection, numerous studies have confirmed the utility of the technique and have greatly expanded its scope as a research tool. For magnetofection, vectors for nucleic acid delivery are associated with magnetic nanoparticles and the delivery process is directed and enhanced by the application of gradient magnetic fields. This procedure sediments the full applied vector dose on target cells in culture within minutes and is suitable to accumulate or retain a vector dose in a target tissue *in vivo*. Magnetofection leads to enhanced cellular uptake, improved dose-response profiles and transfection/transduction kinetics of virtually any vector type (1).

Two types of magnetic nanomaterials are commonly used to magnetize gene delivery vectors. These include functionalized polymeric micro- and nanoparticles with entrapped iron oxide nanoparticles (2,3) and magnetic iron oxide nanoparticles of the core-shell type (4). The assembly of magnetic (nano) particles with nucleic acids or viral particles occurs due to electrostatic and hydrophobic interactions (4) and specific ligand-ligand interactions (2,3,5). The first magnetic core-shell nanoparticles that were designed for gene delivery were transMAG^{PEI} iron oxide nanoparticles that were stabilized with high molecular weight polyethylenimine (PEI) of 800 kD (4). These and other particles that were modified using PEIs of different molecular weights readily associated with lentiviral, retroviral, adenoviral and measles virus vectors and allowed for efficient *in vitro* magnetic transduction (4,6–8). A major limitation in polyethylenimine-mediated gene delivery is dose-dependent cytotoxicity (9–11). Therefore, further optimizations in nanoparticle design and formulation are important objectives in terms of efficiency in gene delivery, cell viability, and in the case of stem cells for the preservation of pluripotency upon magnetofection (1,8,12). The nature of the surface coating components and their arrangement in the surface layer of the nanoparticles were shown to play a crucial role in the efficacy of the magnetic vectors (13,14). Recently we have demonstrated significant effects of nanoparticle coatings on the activity of the adenovirus-magnetic nanoparticle complexes *in vitro* and *in vivo* (15) as well as on the efficacy of gene delivery to Jurkat T cells using non-viral vectors associated with magnetic nanoparticles (16).

Mesoporous silica particles have been developed recently in nanotechnology for drug/gene delivery and biosensing (17,18). Silica coatings are known to result in well stabilized, high quality aqueous suspensions of iron oxide nanoparticles (19,20) and could improve the chemical stability of the nanoparticles and reduce their toxicity (21,22).

Composite silica particles with entrapped magnetite nanocrystals have been engineered (23). The coating of the magnetite "capped" mesoporous silica nanoparticles with 25-kD polyethylenimine and their subsequent association with DNA resulted in the effective transfection of H292 human lung mucoepidermoid carcinoma cells with efficiencies that were superior to those obtained with the Polymag™ and Lipofectamine 2000 systems (24).

We sought to design magnetic core-shell nanoparticles with an iron oxide core that combined the positive characteristics of the silica and polyethylene coatings and that were efficient in gene delivery. We synthesized iron oxide nanoparticles by precipitating Fe(II)/Fe(III) hydroxide in an aqueous solution for their transformation into magnetic iron oxide, followed by the hydrolysis and condensation of tetraethyl orthosilicate (TEOS) to produce siloxane bonds (Si-O-Si) and to promote condensation into the (SiO_x) silica-like coatings of the iron oxide nanoparticles. The co-condensation of 3-(trihydroxysilyl) propylmethylphosphonate (THPMP) yielded a silicon oxide layer with surface phosphonate groups (SiO_x/Phosphonate) and endowed the aqueous suspension with a highly negative electrokinetic potential of the particles as shown schematically in Fig. 1. We further modified these particles by the addition of 5w% of 25-kD branched PEI based on the iron weights of the particles, resulting in a charge reversal. This material, which we have described previously (25), demonstrated high transfection efficiencies *in vitro* as a component of magnetic lipoplexes (25). The lentiviral complexes of the PEI-modified silica-iron oxide magnetic nanoparticles allowed for the excellent transduction of cultured and primary cells as hematopoietic stem cells and human mesenchymal cells in a procedure that we have termed magselectofection (26). Recently, we have shown that the efficiency of an oncolytic adenovirus can be dramatically increased *in vitro* and *in vivo* when combined with PEI-decorated silica-iron oxide nanoparticles (15).

The drawback of this system is that the electrokinetic potentials of the particles titrated with 5w% PEI in the water suspension and colloidal stabilities decrease during storage, resulting in a gradual loss of the magnetofection capacity of the particles. The agglomeration and destabilization of silica nanoparticle suspensions are known to be serious problems (27,28), which can be even more pronounced for magnetic silica-stabilized nanoparticles because of the magnetic dipole-dipole interparticle interactions. Therefore, we have been highly motivated to search for the optimal formulation of PEI-decorated silica iron oxide nanoparticles. Parameters such as surface charge, colloidal stability, association with viral vectors, stability of the complexes at high serum concentrations and transduction efficiencies were used for the optimization of the particle/vector assembly. We have also performed imaging experiments on a clinical 1.5 T MRI system, to evaluate the MRI contrast relaxivities of the free and cell internalized primary silica-iron oxide nanoparticles and the particles that were decorated with PEI.

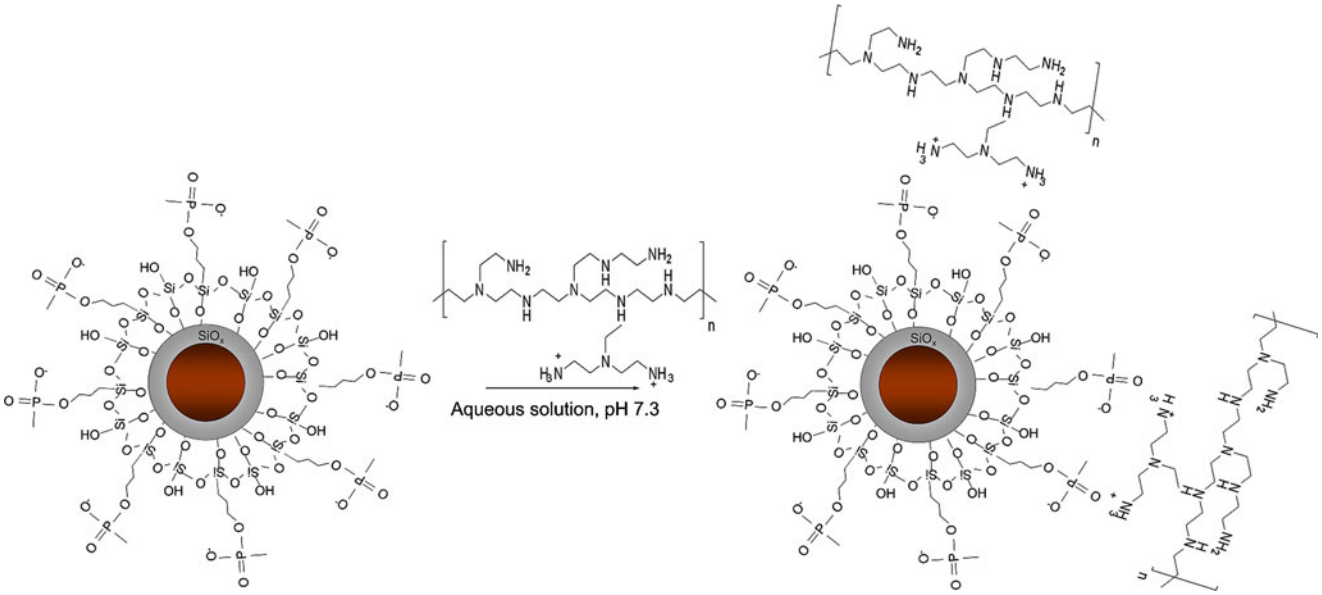

Fig. 1 Schematics of silica-iron oxide magnetic nanoparticles modified for gene delivery. Magnetic iron oxide nanoparticles with a coating resulting from hydrolization and condensation of tetraethyl orthosilicate and 3-(trihydroxysilyl)propylmethyl phosphonate are further "decorated" with 25-kD branched polyethylenimine at different PEI-to-iron *w/w*% ratios *n* yielding the SO-Mag6-*n* particles suitable for association with gene delivery vectors.

MATERIALS AND METHODS

Materials

Dulbecco's modified Eagle's medium (DMEM), L-glutamine, Dulbecco's phosphate buffered saline (PBS), minimal essential vitamins, and 0.25% trypsin/0.02% EDTA solutions were obtained from Biochrom AG (Berlin, Germany). Sodium ^{125}iodide in NaOH was purchased from Amersham Biosciences (New South Wales, Australia), fetal calf serum (FCS) was purchased from PAN-Biotech (Aidenbach, Germany), Triton X-100 was purchased from AppliChem (Darmstadt, Germany), and D-luciferin was purchased from Synchem OHG (Felsberg, Germany). All other chemicals were of analytical grade and used without further purification (Sigma-Aldrich, Steinheim, Germany). Tissue culture plates and flasks were obtained from Techno Plastic Products (Trasadingen, Switzerland). A 96-magnet plate with a permanent magnetic field with a field strength and gradient of 70−250 mT and 50−130 T/m, respectively, which was generated at the cell layer location, was supplied by OZ Biosciences (Marseille, France).

Synthesis and Modification of the Core-Shell-Type Silica-Iron Oxide Magnetic Nanoparticles

Core-shell-type silica-iron oxide magnetic nanoparticles (MNPs) were synthesized as previously described with slight modifications (25) by precipitation of Fe(II)/Fe(III) hydroxide from the aqueous solution of the mixture of Fe(II) and Fe(III) salts followed by transformation into magnetite in an oxygen-free atmosphere. The surface coating resulted from the condensation of tetraethyl orthosilicate (TEOS) and 3-(trihydroxysilyl) propylmethylphosphonate (THPMP), yielding a silicon oxide layer with surface phosphonate groups (SiO_x/Phosphonate). Briefly, 25 mmol (6.8 g) of ferric chloride hexahydrate and 12.5 mmol (2.5 g) of ferrous chloride tetrahydrate in 200 ml ddH_2O water that was filtered using a 0.2-μm filter flask under argon gas were treated with 15 ml concentrated ammonium hydroxide to obtain a primary precipitate. The material was heated to 90°C for 15 min and then stirred at this temperature for 30 min. To form a coating, 375 μl of TEOS (1.7 mmol) was added. After 30 min, 750 μl of 42% THPMP solution (1.3 mmol) was added, and the mixture was further incubated at 90°C for 30 min, cooled to 25°C, diluted two-fold with ethanol, and incubated for 24 h with continuous stirring. The particles were separated by exposure to a gradient magnetic field and washed twice with ethanol and once with water. The product was sonicated for 10 min using a resonance frequency of approximately 20 kHz at 75 mW with impulses applied at 60 s/30 s intervals and dialyzed extensively against water using a Spectra/Por®6 50-kD cut-off dialysis membrane. The MNP suspension was sterilized using ^{60}Co gamma-irradiation at a dosage of 25 kGy.

The decoration of the surface of the SO-Mag5 particles with 25-kD branched polyethylenimine (PEI) at a PEI-to-iron *w/w* ratio of n% resulted in SO-Mag6-n particles with SiOx/Phosphonate-PEI coatings. A sterile-filtered (0.2 μm) PEI solution in water with a pH of 7.3 (HCl) was added to an equal volume of MNP suspension after vortexing to

obtain the required PEI-to-iron ratio. The reagents were mixed in opposite order (MNP suspension into PEI solution) only if indicated.

Physico-Chemical Characterization of the MNPs

Iron Analysis

Iron concentration per unit weight of dry nanomaterials and MNP concentration in the suspensions as related to iron concentration per unit volume were determined spectrophotometrically by forming complexes with 1,10-phenanthroline as described previously (29). The concentrations of the shell components were indirectly calculated from the iron concentrations and accounting for the X-ray diffraction data from the phase composition of the core.

Transmission Electron Microscopy

To activate the grid and to remove hydrocarbon contamination, a formvar/carbon coated 400 mesh copper grid was treated by a hydrogen/oxygen plasma of 50 mW for 30 s (Solarus Model 950, Gatan GmbH). A 5-μL drop of the SO-Mag5 nanoparticle suspension containing 25 μg Fe/ml was placed onto the grid and incubated for 10 min. Samples were rinsed carefully with two drops of double-distilled water and air-dried prior to imaging at an accelerating voltage of 80 kV using a TITAN 80–300 S/TEM (FEI Company).

X-Ray Diffraction

X-ray diffraction patterns were obtained for the powdered sample using a Burevestnik DRON-4-07 diffractometer (St.-Petersburg, Russia) with nickel-filtered CuK$_\alpha$ irradiation. The mean crystallite size $\langle d \rangle$ was calculated from the broadening of the X-ray diffraction (XRD) peaks using the Scherer formula.

Magnetic Structure of the SO-Mag5 Nanoparticles

The static magnetic properties of the SO-Mag5 particles were evaluated by measuring the quasistatic magnetization in the applied DC-fields or M(H) by using the MPMS commercial susceptometer (Quantum Design, USA). The dynamic magnetic properties of the particles were studied by the magnetorelaxometry (MRX) method using a device that was described previously (30). In short, the magnetic moments of the MNPs in a sample are aligned in an external magnetic field of approximately 2 kA/m. After switching off the field, the decay of the magnetization within approximately 500 μs is measured by a low-Tc SQUID at T=295 K.

The relaxation of the non-interacting immobilized MNPs is governed by the Néel relaxation time $\tau_N=\tau_0 \exp\{KV/k_BT\}$ (k_B being the Boltzmann constant), which is determined by the effective anisotropy energy that is represented by the equation $E_A=K\,V$. The observed relaxation of the magnetization is the superposition of the relaxation of the particles with various anisotropy energies. The moment superposition model (MSM) (31) considers the anisotropy constant K to be independent of the particle size and superimposes the relaxation contributions of each size. By fitting the median μ and distribution parameter σ of the lognormal size distribution to the relaxation curve using the MSM, the size distribution can be reconstructed. Note that this size distribution considers the effective magnetic sizes to be equal to the core sizes for proper single domain MNPs that lack magnetic correlations among each other.

Using a similar MSM for the description of the M(H)-data of noninteracting MNPs (32);

$$M(H) = \phi M_S \frac{1}{V} \int_0^\infty f(\mu,\sigma,d)\frac{\pi}{6}d^3 L(d, M_S, T, H)\mathrm{d}d + A_P M_P \tag{1}$$

where L, T, and H denote the Langevin function, temperature, and external field strength, respectively, and using $d=(6V/\pi)^{1/3}$, we fitted μ and σ of the distribution $f(\mu,\sigma,d)$. Here, we added a paramagnetic signal M_P with the arbitrary amplitude A_P (additional fit parameter), representing the magnetization behavior of a non-ferrimagnetic portion of the MNP, which is often denoted as a magnetic "dead layer". Then, the mean diameter corresponding to the volume V of the magnetic portion of a core particle, d_{mV}; i.e., the size of its effective magnetic domain, was estimated. The volume fraction $\phi=1/3\ c_{Fe}M_{M\rho M}{}^{-1}$ was estimated from the density ρ_M and molar mass M_M of the bulk magnetite and iron concentration (c_{Fe}) of the sample, which was determined by Prussian Blue Staining in combination with a light absorption measurement at 690 nm.

Dynamic Light Scattering

The mean hydrodynamic diameter (D_h) and electrokinetic potential (ζ) of the coated MNPs were measured by photon correlation spectroscopy (PCS) using a Malvern Zetasizer Nano Series 3000 HS (Malvern Instruments GmbH, Herrenberg, Germany).

X-Ray Photoelectron Spectra

X-ray photoelectron spectra (XPS) were recorded using a Kratos analytical electron spectrometer (Manchester, UK) that employs monochromated AlKα excitation (1486.6 eV)

and analyzes the elemental composition of the surface coating. The samples were allowed to dry on aluminium foil and measured in the electrostatic-mode. An instrument vacuum of at least 10^{-9} mbar was maintained during the analysis. The relative elemental surface composition was calculated based on the Fe2p peak.

Evaluation of the Stability of MNP Suspensions by STEP-Technology Combined with Multisample Analytical Centrifugation

The time- and space-resolved detection of light transmission (STEP-Technology) combined with multisample analytical centrifugation (LUMiSizer, LUM, Germany (33,34)) was applied for the analysis of the colloidal stability and determination of the particle size distributions of the MNP suspensions (35). The shapes and progressions of the transmission profiles of the MNP suspensions that were measured during centrifugation along the optical cuvette contained the information regarding the state of a dispersion, like flocculation and particle properties. The transmission profiles are representative of the distribution of the particle concentrations over the entire sample length. Based on this, sedimentation and clarification kinetics and the velocity and particle size distributions can be quantified.

Particle-Virus Interaction

Viral Vectors

The third generation, self-inactivating lentivirus vector LVSFeGFP expressing eGFP under control of the constitutive spleen focus-forming virus LTR promoter was produced following a protocol that was established by Wübbenhorst *et al.* (36). The transfer vector pHIV-7SFeGFP was packaged by the transient calcium phosphate co-transfection of 293T cells using a mixture of HIV-1-derived pMD.GP (Gag-Pol), pRSV-rev and the VSV-pseudotyping pMD.G packaging constructs. The harvest containing the viral particles was filtered through a 0.45-μm filter, and the resulting virus stock, with an infectivity of 8.1×10^6 TU/ml, was stored at −80°C in aliquots. The biological titer of the eGFP lentivirus (infectious particles/ml or transducing units/ml=TU/ml) was determined in CMS5 cells as described by Barry *et al.* (37) with modifications. Similarly, the third generation, self-inactivating lentivirus vector LVSFeGFPLuc expressing a fusion protein that consisted of eGFP and firefly luciferase reporters was produced. The stock of the lentivirus contained 1.0×10^9 vector particles (VP/ml) with an infectivity of 1.2×10^6 TU/ml.

An adenoviral vector expressing the chimeric green fluorescent protein fused to HSV1 thymidine kinase (AdV-(TK/GFP)(fus)) that was driven by the mCMV promoter was constructed and kindly provided by Dr. Rodolfo Goya (38) and will further be referred to as the AdV vector. The AdV vector was expanded in 293 cells and purified by double cesium chloride gradient centrifugation according to Hitt *et al.* (39) with modifications, resulting in a virus stock containing 4.3×10^{12} VP/ml and 2.6×10^{11} TU/ml. To determine the virus particle titer (40), the aliquot of the virus stock was diluted 1 to 20 in PBS that contained 0.1% sodium dodecyl sulphate, mixed thoroughly for 2 min and centrifuged at 8000 g for 5 min. The optical density at 260 nm was measured, and the physical virus titer was calculated, taking into account that an OD of 1 corresponds to 1.1×10^{12} VP/ml. Aliquots of the stock were stored at −80°C.

Radioactive Labeling of the Adenovirus

The AdV adenovirus was labeled with radioactive ^{125}iodide as previously described (41). Briefly, 100 μl of the virus stock containing 9.8×10^{10} infectious units per ml and 4.4×10^{12} VP/ml was mixed with 4 μl of sodium ^{125}iodide (1 mCi in 10 μl, Amersham Biosciences) in a iodogene tube (Thermo Scientific Pierce Protein Research Products) and incubated with gentle agitation for 40 min. After adjusting the volume to 500 μL with PBS, the labeled virus was separated from unbound label by gel filtration using a PD-10 column (GE Healthcare) that was preequilibrated with PBS. The product fraction containing 1.23×10^{11} VP/ml with a radioactivity of 2,833 kBq/ml (determined using a Wallac 1480 Wizard 3 automatic gamma counter, Finland) was used to further quantify the virus association with the MNPs.

Adenovirus Association and Magnetic Sedimentation with Magnetic Nanoparticles and Stability of the Complexes in the Presence of FCS

For the binding studies, 50 μl of a 2-to-3 dilution series of the MNPs in ddH_2O (0−60 μg of Fe) were mixed with 250 μl of ^{125}I-labeled AdV suspended in PBS (1.2 VP/ml, 5×10^4 CPM/ml) in a U-bottom 96-well plate at virus concentrations of 1.0×10^9 VP/ml at the time of assembly and incubated for 20 min at room temperature (RT) to form magnetic virus complexes at MNP-to-virus ratios of 0−200 fg of Fe/VP. One hundred fifty microliters of the resulting complexes were transferred into the wells of a new U-bottom 96-well plate containing 150 μl of FCS, followed by gentle mixing and a 30 min incubation. The U-bottom plate was positioned on a 96-magnet plate for 30 min prior to the collection of 50 μl of each supernatant for gamma counting using the gamma counter. The percentages of adenovirus particles that associated and magnetically sedimented with the MNPs in PBS or 50% FCS were calculated as described in (41).

Cell Culture

SH-SY5Y human neuroblastoma cells that were used for the *in vitro* experiments (further referred to as SH-SY5Y cells) were grown in DMEM supplemented with 15% FCS (Gibco), 2 mM L-glutamine and 1% non-essential amino acids. McA-RH7777 rat hepatocellular carcinoma (HCC) cells obtained from the ATCC (LGC Standards GmbH, Wesel, Germany), CMS5, 293 and 293T cells were cultured in Dulbecco's modified Eagle medium (DMEM) (Gibco) that was supplemented with 10% heat-inactivated FCS (Gibco), 1% non-essential amino acids (PAA), 100 U ml^{-1} penicillin (PAA), and 100 μg ml^{-1} streptomycin (PAA). This medium will hereafter be referred to as the cell culture medium. Mouse pancreatic ductal adenocarcinoma cells were extracted as primary cells from a CKp53lox mouse ($Ptf1a^{wt/Cre}$; $Kras^{wt/LSL\text{-}G12D}$; $p53^{fl/fl}$) by Marija Trajkovic-Arsic, II. Med. Clinic, Gastroenterology, Klinikum rechts der Isar, Technische Universität München (referred to as 511181 cells) and were cultured in the same cell culture medium. The cells were grown at 37°C in a humidified atmosphere containing 5% CO_2.

Magnetotransduction Efficiency with Lentiviral Magnetic Vectors of the Silica-Iron Oxide MNPs Decorated with PEI

Magnetotransduction In Vitro

SH-SY5Y cells were seeded into a 96-well plate at a density of 20,000 cells per well. For the lentiviral magnetotransduction that was conducted 24 h later, 50 μl of 2-fold serial dilutions of the magnetic complexes of the lentiviral vector LVSFeGFPLuc were added per well. To prepare the SO-Mag6-n/LVSFeGFPLuc magnetic complexes, 72 μl of the virus stock were mixed with 6 μl of the SO-Mag6-n stock (100 μg Fe/ml) and kept at RT for 20 min to allow for complex assembly followed by a dilution to 360 μl with DMEM (without additives), resulting in MNP:VP ratios of 10 fg Fe/VP, 6×10^7 VP/ml and 7.2×10^4 TU/ml. The complexes were freshly prepared before use. A magnetic field was applied by positioning the cell culture plate into the 96-well magnetic plate for 30 min.

Evaluation of the Reporter Gene Expression

To evaluate the transfection efficiency in terms of the percentage of eGFP-positive cells, we washed the cells twice with PBS supplemented with 1% FCS (hereafter referred to as FACS buffer) at 48 h post-transfection, fixed the cells using the Cytofix™ Fixation Buffer (Becton Dickinson) and resuspended the cells in 0.5 ml of FACS buffer for the FACS analysis using the FACSVantage™ device (Becton Dickinson, with an argon laser excitation maximum at 488 nm; fluorescence was measured using a 530/30-nm bandpass filter). At minimum, 20,000 events per sample were analyzed. The luciferase expression assay on the cell lysate was performed as described elsewhere (29).

Infectivity of the Magnetic Lentiviral Complexes over the Course of Storage

To assess the changes that occurred in the infectivity of the magnetic lentiviral complexes during storage, the magnetic complexes of the SO-Mag6-10 particles with the self-inactivating lentivirus vector LVSFeGFP in addition to the complexes with polybrene (PB) were prepared and stored in 250 μl aliquots at −4°C or −80°C until the titer determination in the CMS5 cells, which was carried out at days 2, 37, 72, 149 of storage. The complexes will be further referred to as SO-Mag6-10/LV and PB/LV. Complexes that were freshly prepared each time just prior to infection (SO-Mag6-10/LV and PB/LV) were used as references. To prepare the SO-Mag6-10/LV magnetic complexes, 2,000 μl of the LVSFeGFP stock (8.1×10^6 TU/ml and 7.8×10^9 VP/ml) were mixed with 16 μl of the SO-Mag6-10 stock (5 mg Fe/ml) and kept at RT for 20 min to allow for complex assembly and divided into 250 μl aliquots to be stored or immediately used for cell transduction. Similarly, 2,000 μl of the LVSFeGFP stock were mixed with 20 μl of PB stock solution in water containing 800 μg PB/ml.

For the titer determination, the CMS5 cells were seeded into a 12-well plate at a density of 100,000 cells per well. After 24 h, the medium was removed, and 250 μl/well of serial dilutions of the SO-Mag6-10/LV complexes with the cell culture medium or of the PB/LV complexes in cell culture medium containing 8 μg PB/ml were applied. After 2 h, 1 ml cell culture medium per well was added, and the cells were further incubated for 48 h until sampling for the FACS analysis. The percentage of eGFP-positive cells was plotted against the $\log_{10}$ of the applied volume of the virus stock per cell. The dose-response curves were fitted with logistic functions using the OriginPro 8G software. The virus titer was calculated assuming that the virus dose resulting in 50% reporter-positive cells corresponded to 0.5 TU/cell.

Particle-Cell Interaction

Cell Labeling with MNPs

SHSY5Y human neuroblastoma cells were seeded at a density of 700,000 cells per well in a 6-well plate. HCC and 511181 cells were seeded at a density of 500,000 and 200,000 cells per well, respectively. At 24 h post cell seeding, the cell culture medium of each well was changed to a MNP

suspension. The MNPs were diluted in cell culture medium to achieve the desired applied iron dose per cell. A range of 2–60 μg Fe ml^{-1} was used for the SHSY5Y cells, resulting in an iron dose of approximately 7.5 to 240 pg Fe/cell. A range of 12.5–100 μg Fe ml^{-1} was used for the hepatic cells and 5–80 μg Fe ml^{-1} for the 511181 cells, resulting in an applied iron dose of approximately 25 to 400 pg Fe per cell in a 1 to 2 dilution series. After a 24 h incubation, the cells were washed with PBS and incubated with 100 units ml^{-1} of a heparin solution that was added to the cell culture medium for 20 min at 37°C to dissociate any loosely bound nanoparticles. Next, the cells were washed with PBS and trypsinized using a 0.25% trypsin/0.02% EDTA solution to analyze the associated/internalized iron.

Based on the results of the saturation curves (Fig. 9b), cells were labeled for the preparation of MRI phantoms. HCC cells were seeded at a density of 80,000 cells per cm^2 in a 75 cm^2 dish, while 511181 cells were seeded at a density of 46,667 cells per cm^2 in a 75 cm^2 dish. At 24 h post-cell seeding, the SO-Mag6-11.5 particle suspension in the cell culture medium was applied at a dose of 100 pg Fe $cell^{-1}$. The MNPs were incubated with the cells for 24 h, washed twice with PBS to dissociate any loosely bound nanoparticles and trypsinized. After washing with PBS, the cells were fixed with BD Cytofix™ (BD Biosciences), washed three times with PBS and stored at 4°C in PBS/0.5% NaN_3 until their use in further analyses. The cells that were used to prepare the calibration phantoms for MRI imaging were loaded with 39 and 27 pg Fe/cell for the HCC and 511181 cells, respectively, for the analysis of exogenic non-heme iron, which was performed as described below.

Analysis of Cell-Associated/Internalized Iron

For the analysis of the exogenic non-heme iron from the cell-associated/internalized MNPs, the analysis of the non-heme iron concentrations of the MNP-labeled cells was performed as described elsewhere (42). Briefly, approximately 200,000 trypsinized cells were washed with PBS and then spun down by centrifugation. The supernatant was discarded, and the cell pellet was resuspended in 250–500 μl of an acid mixture containing 3 M HCl and 0.6 M trichloracetic acid. After an overnight incubation at 65°C, the samples were centrifuged, and 50 μl of the clear supernatant was analyzed for its iron concentration by a colorimetric method with 1,10-phenanthroline as previously described (29). Basal non-heme iron levels that were determined in non-labeled cells were used as references.

Cytotoxicity Evaluation

The MTT assay, based on the reduction of the MTT reagent into formazan by superoxide anion radicals that are produced in the mitochondrial respiratory chain (43), was carried out as described previously (29) to assess the cytotoxicity of the MNPs. Briefly, SHSY5Y cells were seeded at a density of 20,000 cells per well in a 96-well plate. At 24 h post cell seeding, the cell culture medium of each well was changed to a MNP suspension. After 48 h incubation with MNPs, cells were washed once with PBS, the supernatant was discarded, and the cells were incubated for 1–2 h in 100 μl of 1 mg/ml MTT solution that was prepared in Hank's balanced salt solution with 5 mg/ml glucose. Afterwards, 100 μl solubilization solution (10% Triton X-100 and 0.1 N HCl in anhydrous isopropanol) was added and incubated at 37°C overnight with shaking to dissolve the formazan. The optical density was measured at 590 nm. Untreated cells were used as references.

Evaluation of MRI Contrast Efficiency of MNPs

Calibration Phantoms for MR Imaging

Calibration phantoms of the MNPs and MNP-labeled cells for MR imaging were prepared in 24-well plates. Sample and background wells were arranged in an alternating order to avoid signal interference of different samples. In addition spaces in-between wells were filled to avoid signal interference from air. The background wells and spaces between the wells were filled with an agarose gel of a tissue-mimicking composition. According to Christoffersson *et al.* (44), tissue-mimicking phantom material can be prepared by using different concentrations of nickel and agarose. Increasing the nickel (II) ions concentration shifts the T_1 values to longer relaxation times, and increasing agarose concentrations results in shorter T_2 relaxation times (44). The gel phantom-mimicking relaxivity of the rat liver tissue (T_1=550 ms and T_2=48 ms) was prepared with 198 mM $Ni(NO_3)_2$, 2.45% agarose and 0.5% sodium azide. The gel phantom mimicking the mouse pancreatic ductal adenocarcinoma (mPDAC) tissue with relaxation times of T_1=1200 ms and T_2= 115 ms was prepared with 0.53 mM $Ni(NO_3)_2$, 1.01% agarose and 0.5% sodium azide. The 12 background wells and cavities between the wells on the upside and bottom were filled with the described Ni-doped agarose gel.

For the 12 sample wells, a gel containing a 1.5-fold concentration of nickel and agarose was prepared, which is further referred to as the internal agarose gel. A 2 to 3 dilution series in water, beginning with 72 μg Fe/ml (1.3 μM Fe) as the highest iron concentration, was prepared for both the particles and labeled cells.

The maximum final cell concentration of the liver phantoms was 6.2×10^5 cells ml^{-1}, and was 8.6×10^5 cells ml^{-1} for the

mPDAC phantoms, accounting for the MNP loading of 39 and 28 pg Fe/cell for the McA-RH7777 rat hepatocellular carcinoma and 511181 mouse PDAC cells, respectively. The dilutions of the MNPs or MNP-labeled cells and the internal agarose gel were pre-warmed at 65°C. Then, 1.5 ml MNP dilution were vortex-mixed with 3 ml internal agarose gel in a 15-ml falcon tube to distribute the material homogenously and avoid air bubbles and transferred into the according well. The plate was allowed to cool down slowly and was sealed with paraffin to avoid the evaporation of water during storage at 4°C.

MR Imaging Experiments

All of the imaging experiments were performed using a clinical 1.5 T MRI system (1.5 T Achieva, Philips Medical System, Best, The Netherlands) with the 8-channel SENSE head coil for signal reception. T_2 and T_2^* maps of the calibration phantoms were measured using the following sequences: for T_2, a multi spin echo sequence with T_R= 2,000 ms, TE=n * 4.9 ms (n=1…30), flip angle=90°, FOV=160×88, resolution=1×1×3 mm^3, 3 slices of 3 mm thickness with no gap and a total scan time of 6:04 min, and for T_2^*, a multi-echo gradient echo sequence (FFE) with T_R=1,000 ms, TE=2.1+n * 3.2 ms (n=0…15), flip angle=90°, FOV=160×92, resolution=1×1×3 mm^3, and 3 slices of 3-mm thickness with no gap and a total scan time of 4:40 min.

T_2 maps were calculated from the multi spin-echo data using the standard MR scanner mono-exponential fitting routine. For the T_2^* maps, the complex data of the multi-echo gradient-echo sequence were analyzed using the RelaxMapsTool from the Philips PRIDE data evaluation software package. This tool calculates B_0 maps for all slices and, as a first order deviation from a mono-exponential signal decay, takes into account the sink-shaped oscillation of the multi echo signal that is induced by the through plane B_0 gradient (45).

The rectangular agarose phantom plates were centrically positioned on the head cushion of the coil. For the analysis, circular regions of interest (ROIs) were manually chosen for each well, and the mean (± standard deviation) R_2 and R_2^* values were calculated from the T_2 ad T_2^* values. The mean R_2^* values were plotted against the MNP concentrations and/or the iron concentration to determine the corresponding transverse relaxivities (r_2^*, $s^{-1}(mM\ Fe)^{-1}$) by linear regression.

Statistical Analysis

The results are expressed as the mean ± standard deviation (SD).

RESULTS

Physico-Chemical Characteristics of Silica-Iron Oxide MNPs

The iron concentration of the silica iron oxide SO-Mag5 MNPs was 0.52 g iron per g dry weight, suggesting, accounting for the phase composition of the core described below, that the coating concentration was 0.28 g matter per g dry weight. The hydrodynamic diameter that was measured in the aqueous suspension was (40±14) nm. The electrokinetic potential was highly negative at −38.0±2.0 mV.

A representative TEM image of the particles is shown in Fig. 2a. The evaluation of the TEM image reveals that the iron oxide core of the particles has an average diameter of (6.7±1.5) nm (Fig. 2b). This is similar to the average crystallite size of 6.8 nm, which was determined from X-ray powder diffraction patterns using the Scherrer formula (Fig. 2d). All of the reflections in the electron diffraction patterns (Fig. 2c) and XRD patterns can be indexed according to cubic magnetite.

Data on quasistatic magnetization, M(H), and magneto-relaxometry (MRX) data for the SO-Mag5 nanomaterial are given in Fig. 2e and f. By fitting (1) to the measured $M(H)$ data (Fig. 2e), we have obtained the mean magnetic volume diameter d_{mV}=(7.3±0.6) nm and distribution parameter σ=0.44±0.01 for the effective magnetic sizes that represent the mean core size of a single MNP domain. The saturation magnetization M_S=(362±10) kA/m=49 Am^2/kg=94 Am^2/kg(Fe) (estimated from the M(H) curve using Eq. 1) refers to the whole particle core volume and is lower than the saturation magnetization of bulk magnetite ($M_{S,bulk}$=480 kA/m=92 Am^2/kg=127 Am^2/kg (Fe) (46)). A reduction in the magnetization compared to the bulk material $M_{S,bulk}$-M_S may be due to the partial oxidation of the core material into maghemite, for which $M_{S,bulk}$=(340–390) kA/m (47). However, it may also result from the so called magnetically "dead layer" at the surface of the nanoparticles that can be thought of as a transition layer between a coating material and the magnetically active region of the particle core (48). The magnetically dead layer could be chemisorption induced (49) or result from a surface spin disorder (50), which is typical for magnetic nanoparticles that are smaller than the critical diameter and have high surface-to-volume ratios (51). This is supported by the poor saturation behavior of $M(H)$ in Fig. 2e.

The fitting of the MRX curve (Fig. 2f, freeze dried sample) resulted in a core magnetic diameter of (6.4±1) nm and σ=0.35±0.04, where an anisotropy constant of K=(6±3) kJ/m^3 was found. The hydrodynamic size d_{VC} that was evaluated from the MRX curve for the liquid suspension (Fig. 2f) was (95±14) nm with the related distribution parameters σ=0.57±0.04.

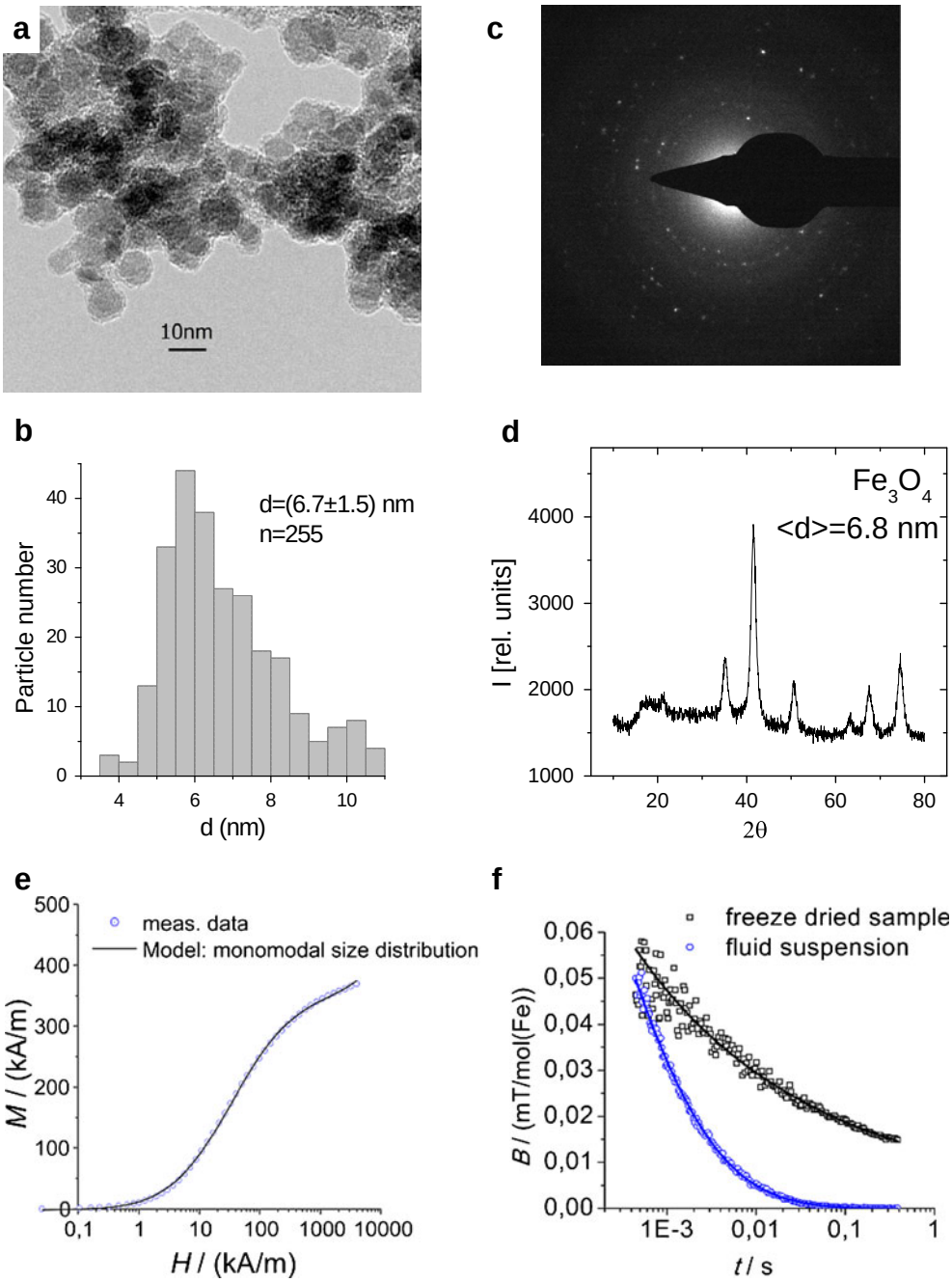

Fig. 2 Morphology, phase composition and magnetic structure of the core of the SO-Mag5 nanoparticles. The X-ray photoelectron spectrocopy data were moved to the supplementary materials (Figure s2) during the review process. (**a**) Transmission electron microscopy image and (**b**) derived data on the diameter of the core, (**c**) electron diffraction and (**d**) X-ray diffraction patterns. (**e**) M(H) curve and (**f**) MRX-data of fluid aqueous suspension and of a suspension after freeze drying in 10% mannitol (preserving the overall volume of the sample).

XPS is an excellent analytical method for characterizing surfaces. High-resolution X-ray photoelectron spectra provide the elemental surface composition and resolve the oxidation states of individual elements. Fragments of the XPS spectra of the SO-Mag5 nanoparticles are shown in Figure S1, and data on the relative elemental compositions of the surface are given in the Figure table. The phosphor-to-silicon elemental ratio of 1.23 to 4.96, accounting for a phosphor-to-silicon ratio of 1 to 1 in a structural formula of THSMP ($C_4H_{12}NaO_6PSi$), allows for the assignment of 1.23 atomic percent Si to the product of the THSMP condensation. The remaining 3.73% silicon belongs to the product of the TEOS condensation in the surface layer or SiO_x. Taking into account the molecular weight of THSMP (238.18), the average number of phosphonate groups was estimated to be ~1.5 x10^{21} groups per g coating weight.

For a 6.7 nm magnetite particle core, the average weights of the particle and coating are 6.2×10^{-19} g Fe and 3.4×10^{-19} g of coating material per particle. Therefore, there is on average approximately 500 phosphonate groups per particle. Assuming that the density of the silica coating material is 2 g/cm^3, the volume of the silica coating on the surface is approximately 170 nm^3, which gives a thickness of

approximately 1 nm for the coating layer at the surface of the 6.7-nm iron oxide nanoparticles. This value is consistent with the TEM data shown in Fig. 2a. The total diameter of the particle (core plus coating) is ~8.7 nm, and thus the average outer surface of the particle is ~60 nm^2 (or 97 m^2/(g Fe)), and the surface density is ~8.4 phosphonate groups per nm^2 (~13.3 μmol m^{-2} or 1.3 mmol/(g Fe). This high surface density of the phosphonate groups ensures a rather high electrokinetic potential of the particles (−38.0±2.0 mV) when measured in aqueous suspension.

Decoration of Silica-Iron Oxide Nanoparticles with Polyethylenimine and Electrokinetic Potentials and Stabilities of Aqueous Suspensions as Evaluated by STEP-Technology

The decoration of the surface of the SO-Mag5 particles with PEI at a PEI-to-iron *w*/*w* ratio ranging from 1 to 12 w% resulted in SO-Mag6-n particle series with SiO_x/Phosphonate-PEI coatings. We investigated the relationship between the amount of PEI that is added to the nanoparticles, the electrokinetic potential, the particle size distribution, the dispersion stability and the sedimentation behavior.

Increasing the amounts of PEI that were loaded onto particles caused a gradual shift of the surface charge to occur, which changed from a highly negative electrokinetic potential of (−38.0±2.0) mV for primary particles in the aqueous suspension (n=0) to almost neutral particles at 1-2% PEI with increasing positive potentials for higher n-values up to about +40 mV at PEI loading levels of n=5; a saturation at this potential of up to n=12 was observed (Fig. 3a). Neutralization of the surface charges resulted in the aggregation/flocculation of the particles with increased effective hydrodynamic diameters, according to the DSL measurements (Fig. 3b). At PEI loading levels of higher than 5w%, no visual differences in the appearance of the suspensions were observed with the naked eye.

The dispersion stability was quantified by multisample analytical centrifugation with photometric detection. This approach allows for the *in situ* recording of space- and time-resolved extinction (concentration) profiles for the entire sample, measuring from the bottom to the top of the cuvette during centrifugation. Figure 3c shows the transmission profiles for the SO-Mag5 and SO-Mag6-n samples that were obtained during centrifugation for 43 min at 36*g*. As can be observed from the time course of the transmission profiles in Fig. 3c-1, at the beginning of the separation process, particles and aggregates (small flocs) have enough space to separate individually (polydisperse sedimentation). Later, a sharp front of sedimenting particles is formed. Inside a particle network, all of the particles are moving with the same velocity (zone sedimentation). The distance between consecutive profiles narrows because the resistance against further compaction increases with particle concentration inside the network. Behind the sharp front, a gradual increase in transmission is observed, which is related to slowly settling individual fines that are not bound to the particle network; i.e., the dispersion contains larger flocs and fines (primary particles and/or small aggregates). As expected, the characteristics of the transmission profiles change with the PEI-to-iron ratios.

For the undecorated sample (SO-Mag5), only minor changes were observed (Fig. 3c-0). A small degree of polydisperse sedimentation can be traced to just below the filling height (meniscus) because the average particle size is much smaller than that of SO-Mag6-1. By doubling the amount of PEI (SO-Mag6-1→SO-Mag6-2, Fig. 3c-2), the separation mechanism changes to purely zone sedimentation. The flocs settle rapidly, forming a flocculated particle network. There is no residual turbidity, indicating that there is no sign of the separate settling of a fine fraction. In other words, near the IEP, all of the particles are incorporated into the flocs/network.

Further doubling of the PEI concentration (SO-Mag6-2→SO-Mag6-4) again changes the separation mechanism. As shown in Fig. 3c-4, the polydispersity sedimentation of fines behind the sharp front is again obvious. Compared to SO-Mag6-1 (Fig. 3c-1), the sedimentation of the fines is much slower. Further increases in the PEI-to-iron ratios lead to continuous increases in the fraction of the fines and consequently in the turbidity of the supernatant, until the flocculated fraction disappears and zone sedimentation is no longer traceable (Fig. 3c-10 and c-12).

The appearance of the samples after centrifugation is documented in Fig. 4c. The dependence of the sediment height on the PEI-to-iron ratio is shown in Fig. 4a, and the related change in turbidity of the supernatant is quantified by the transmission, which is averaged in the middle part of the sample cell (118–120 mm, Fig. 4b). The sediment height is largest for SO-Mag6-2 particles, and the transmission is highest for SO-Mag6-3 particles (highest degree of flocculation, no fines remaining). With greater PEI concentrations, the sediment height decreases, and the turbidity in the supernatant increases. The same is obvious from the transmission profiles and can be quantified accordingly. The effect of the surface decoration of SO-Mag5 on the size distribution for the varying PEI-to-iron ratios is summarized in Fig. 4d. The primary material has 95% of particles that are smaller than 40 nm. Loading with 1% PEI per mass of iron results in a coarse fraction between 2 and 5 μm; however, this also contains approximately 10% of a broadly distributed fine fraction between 100 nm and 2 μm. At 2% or 3% PEI (a similar curve), the amount of the fine fraction is reduced. After this point, a pronounced bimodality is observed that contains a mix of aggregates that are smaller than 100 nm and larger than 2 μm.

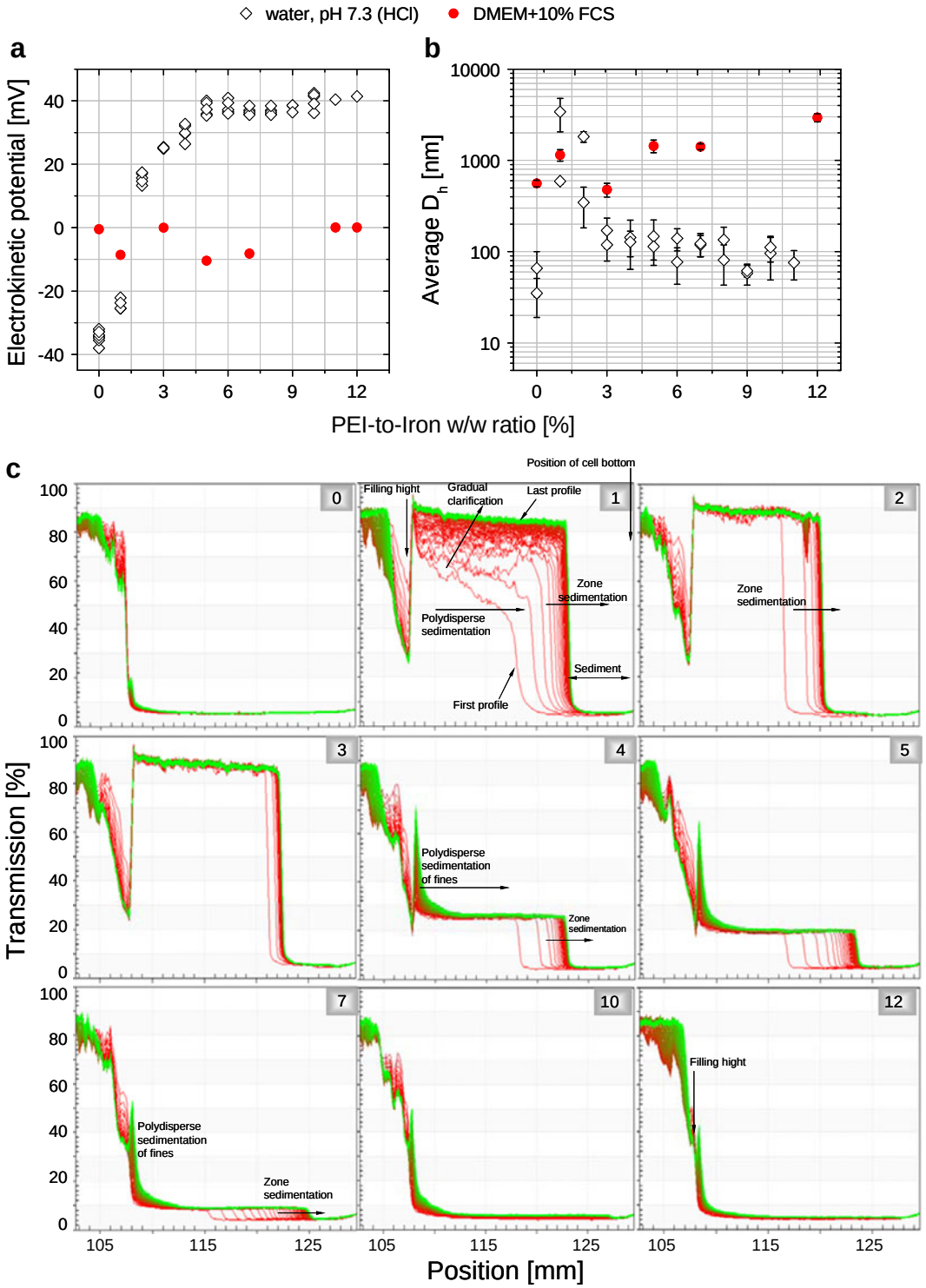

Fig. 3 Characteristics of the aqueous suspensions of silica-iron oxide nanoparticles decorated with polyethylenimine at different PEI-to-iron *w/w* ratios. (**a**) Surface charges and (**b**) hydrodynamic diameter as measured in water suspension or after dilution in DMEM medium containing 10% FCS. (**c**) Stability as evaluated by the time- and space-resolved detection of light transmission (STEP-Technology) combined with multisample analytical centrifugation. The evolution of the transmission profiles as registered in multiple points along the cuvette is displayed for different time points during the course of centrifugation of aqueous suspensions of the SO-Mag5 particles and the SO-Mag6-*n* particles that were titrated with PEI at different PEI-to-iron *w/w*% ratios *n* (*n* values are shown in the grey quadrates at the right bottom corner of the figure); centrifugation was conducted for 43 min at 20°C and 500 rpm (36*g* at the bottom of the cuvette). The position of the filling height is approximately 107.5 mm, and the position of the cuvette bottom is at 129.5 mm.

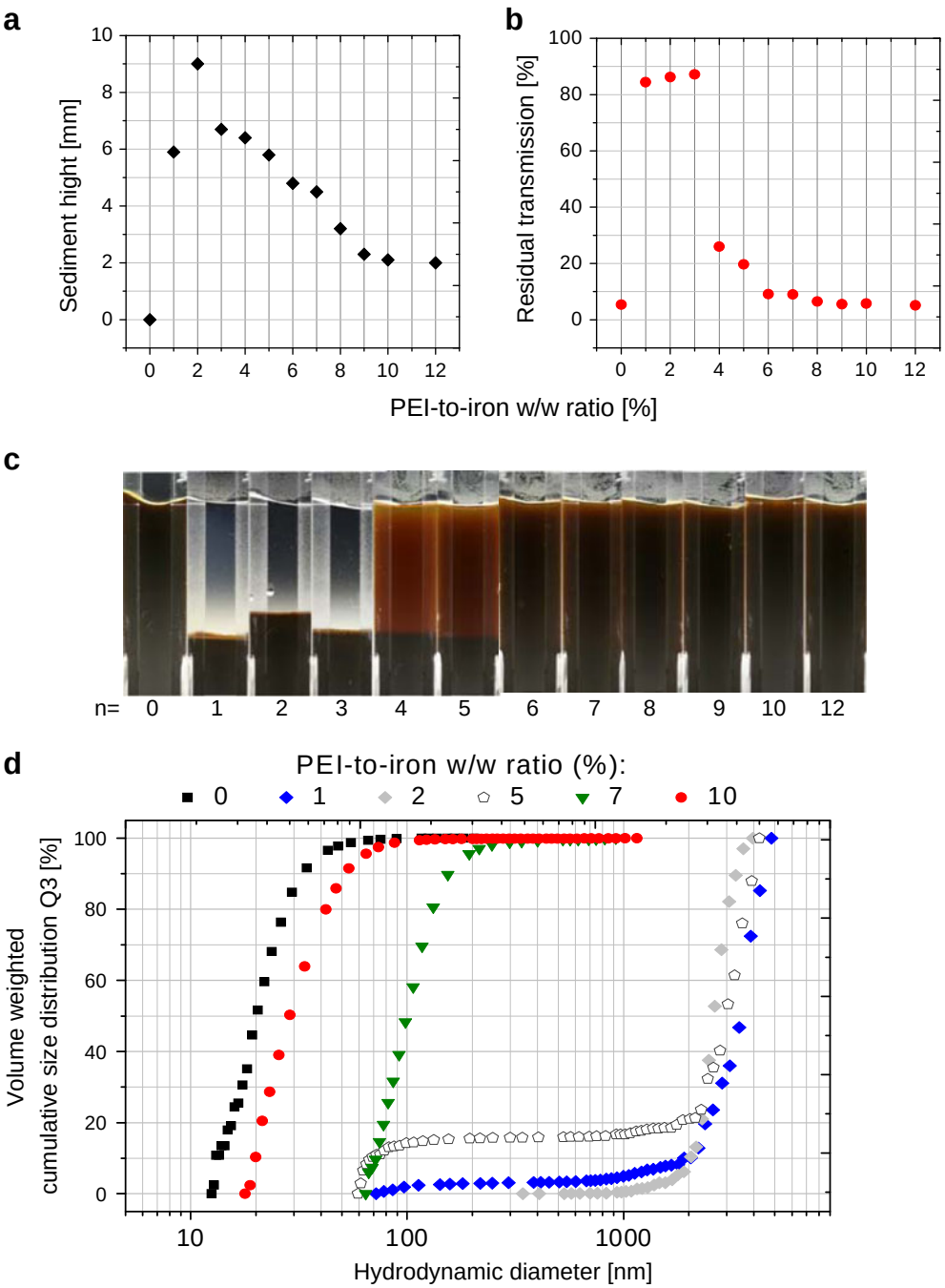

Fig. 4 Parameters of stability for the aqueous suspensions of silica-iron oxide nanoparticles decorated with polyethylenimine. (**a**) Sediment height and (**b**) average transmission in the supernatant (118–120 mm) for aqueous suspensions of the SO-Mag5 particles and the particles that were titrated with PEI at different PEI-to-iron *w/w*% ratios *n*; centrifugation was conducted for 43 min at 20°C and 500 rpm (36*g* at the cuvette bottom). (**c**) Visual appearances of the samples after centrifugation. (**d**) Volume-weighted cumulative hydrodynamic diameter distributions derived from the transmission profiles shown in Fig. 3c.

Beyond SO-Mag6-7 and at higher PEI loading concentrations, the distributions are shifted towards those of the original undecorated sample. Samples loaded with 10–12% PEI kept highly positive electrokinetic potential, colloidal stability and magnetofection potential during storage. Thus, loading with 10% PEI resulted in an average particle hydrated diameter of (89 ± 48) nm and zeta potential of (40.2 ± 0.6) mV. After 12 months storage at 4°C, an average particle hydrated diameter of (69 ± 33) nm and zeta potential of (49.5 ± 0.3) mV were measured for the same SO-Mag6-10 nanoparticles.

When the order of reagent mixing is changed from the addition of PEI into the SO-Mag5 dispersion to the addition of the primary SO-Mag5 particles into the PEI solution, the PEI-to-iron ratio at which there is maximum flocculation does not change; however, the dispersion properties at higher concentrations of PEI are modified. Fig. S2c documents the appearance of the samples after centrifugation for this case. Turbidity in the supernatant is markedly reduced (Fig. S2b), and the sediment is higher (Fig. S2a); i.e., a higher degree of flocculation is preserved compared to

that which occurs when PEI is added to the suspension of the undecorated sample (Fig. 4a and b), despite the fact that the PEI concentrations are the same.

Magnetic Sedimentation of Adenovirus Associated with MNPs and Stability of Resulting Complexes

As shown in Fig. 5a, the amount of adenovirus that associated and magnetically sedimented with the MNPs in PBS increased with increasing MNP-to-VP ratios in terms of iron weight per VP. A maximum adenovirus binding and sedimentation rate of approximately 90% of the initial virus particles was observed at MNP-to-virus ratios higher or equal 5 fg of Fe/VP for SO-Mag6-n particles, n=5–12%. At lower PEI-to-Iron w/w ratio of 3% a maximum adenovirus binding and sedimentation rate of about 75% was observed only at high MNP-to-virus ratios >100 fg Fe/VP. The complexes of AdV that were formed with the SO-Mag6-n particles, n=7 and 12%, at MNP-to-virus ratios of 3–20 fg Fe/VP remained stable after 30 min of incubation in the presence of 50% FCS followed by 30 min of sedimentation on the magnetic plate (Fig. 5b). When the complexes formed with the particles decorated with 5 and 3 w% PEI were incubated in 50% FCS for 30 min, partial destabilization of the adenovirus−MNP complexes occurred (Fig. 5b, right). It is of note that at high serum protein concentrations, up to 75% of the adenovirus was still magnetically sedimented with SO-Mag6-5 nanoparticles at MNP-to-virus ratios >5 fg of Fe/VP, whereas only about 40% of the adenovirus was magnetically sedimented with SO-Mag6-3 complexes even at ratios of higher than 50 fg of Fe/VP.

The complexes of AdV that were formed with the SO-Mag6-n particles, n=7 and 12%, at MNP-to-virus ratios of 10–20 fg Fe/VP (Fig. 5c, left) and 3–5 fg Fe/VP (Fig. 5c, right) remained stable for at least 30 min of incubation followed by 30 min of sedimentation on the magnetic plate both in PBS and 50% FCS. At lower PEI-to-iron ratios

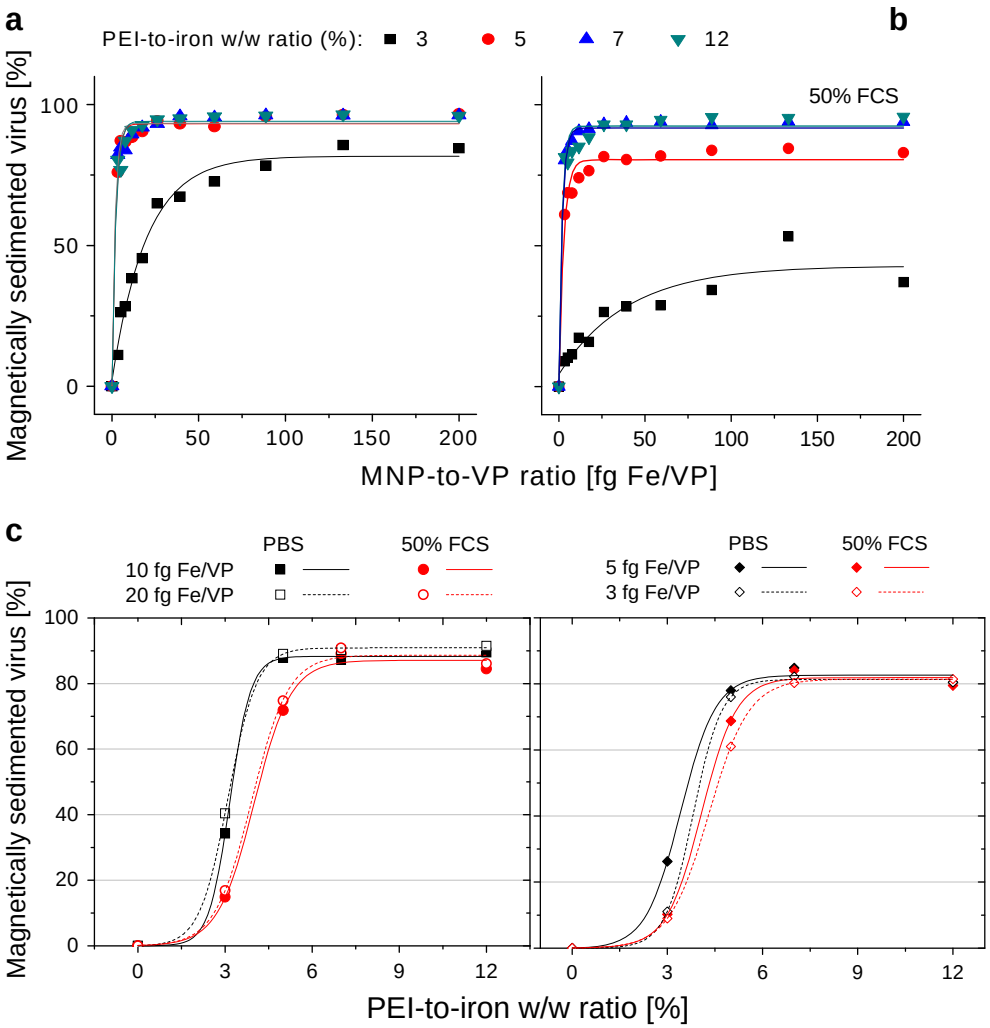

Fig. 5 Particle-Virus interactions. Magnetic sedimentation of the AdV adenovirus associated with the silica-iron oxide nanoparticles decorated with polyethylenimine and the stability of the resulting complexes in 50% FCS. (**a** and **b**) I^{125}-labeled AdV virus and silica-iron oxide nanoparticles decorated with PEI at different PEI-to-iron *w/w* % ratios *n* (SO-Mag6-n nanoparticles, n=3, 5, 7, and 12) were mixed with PBS at various nanoparticle-to-virus particle ratios in relation to the fg of Fe/VP and incubated for 20 min for the complex formation. The resulting complexes were diluted 1 to 1 with PBS (**a**) or FCS (**b**) and then incubated for 30 min before being positioned on the 96-magnet plate for 30 min for the magnetic sedimentation. The I^{125} radioactivity of the supernatants was measured to quantify the percentage of virus that associated and magnetically sedimented with the MNPs. (**c**) The data from Figures **a** and **b** for fixed nanoparticle-to-virus particle ratios of 3.4, 5, 10 and 20 fg of Fe/VP are plotted against the PEI-to-iron *w/w* % ratios of the nanoparticles.

of 3 and 5% even an increase in MNP-to-VP ratios till 200 fg Fe/VP did not ensured sufficient association and magnetic sedimentation of viral particles and stability of the complexes in the presence of high serum concentration (Fig. 5a and b). Therefore, the range of loading of the SO-Mag5 nanoparticles with PEI (7–12%) combined with adequate MNP-to-VP ratios (preferably 10–20 fg Fe/VP) that enabled the adenoviruses to be highly associated with the MNPs and the stability of the complexes in 50% FCS allow for the construction of potentially efficient magnetic complexes for *in vitro* and *in vivo* infections. In concordance with these results, the adenoviral magnetic vectors with SO-Mag6-12.5 nanoparticles that were formulated at 5 and 10 fg Fe/VP at MOI of 2.5 and 5 showed transduction efficiencies in the HUVECs that were more than two orders of magnitude higher in terms of luciferase reporter expression (ng luciferase/μg total protein) compared to the non-magnetic vectors (52).

Magnetotransduction Efficiency with Lentiviral Magnetic Vectors of Silica-Iron Oxide MNPs Decorated with PEI

Previously, we have found that lentiviral particles are also efficiently bound and magnetically sedimented with silica iron oxide magnetic nanoparticles that are titrated with 5% PEI, and the resulting complexes that are constructed at 2–20 fg Fe/VP efficiently transduce primary hematopoietic and mesenchymal stem cells (26). For example, at a lentiviral MOI of 5 and low cell density of 1.5×10^5 cells/mL, 21% of hCB-CD34$^+$ cells were transduced with an eGFP reporter and maintained their progenitor cell phenotype after magselectofection compared to only 0.15% transduction using standard infection protocol at the same cell density. Lentiviral magselectofection with low MOIs (≤3) yielded up to 50% transduction of mouse Lin$^-$Sca1$^+$ cells, which persistently reconstituted T and B cells in *Il2rg*$^{-/-}$ mice, compared to less than 10% transduction with higher MOIs using a standard transduction protocol for Lin$^-$ bone marrow cells.

To identify the PEI loading of the nanoparticles that enables the maximal transduction efficiency, we tested the lentiviral complexes of the SO-Mag6-n particles ($n\leq12\%$) in SHSY5Y human neuroblastoma cells at low applied virus doses per cell (MOI of 0.03–0.5). The results obtained from the luciferase reporter expression that are shown in Fig. 6 clearly indicate the PEI loading of 9–12w% to be optimal in achieving high magnetotransduction efficiency.

Storage Stability of Lentiviral Magnetic Complexes

We tested the lentivirus titer in the CMS5 cells for the SO-Mag6-10 nanoparticle complexes and compared the results with the titer that was determined using the conventional procedure of infection in the presence of 8 μg polybrene per ml medium (polybrene complexes, PB/LV). No magnetic field was applied during the infection. The dose response curves were fitted to quantify the dose that resulted in 50% transduced cells and derived virus titers (Fig. 7a). Freshly prepared complexes were tested in addition to complexes that had been prepared and stored at −80°C or 4°C at different time points during the 5 month storage. The results presented in Fig. 7b show that even in simple-to-transduce CMS5 cells without the application of the magnetic field, the freshly prepared magnetic complexes yielded approximately 2-fold higher transduction efficiencies. One of the reasons for this could be the more efficient internalization of the magnetic complexes even without the application of the

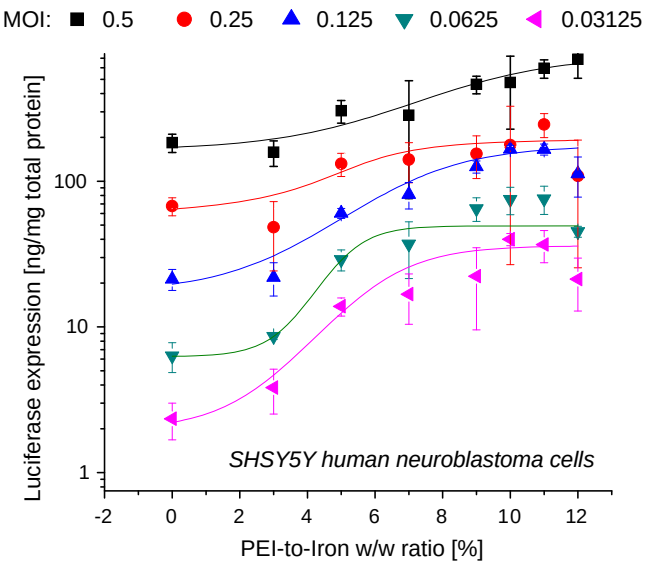

Fig. 6 Magnetotransduction efficiencies of the lentiviral magnetic vectors of the silica-iron oxide MNPs decorated with PEI. SHSY5Y human neuroblastoma cells were transduced with magnetic SO-Mag6-n/LVSFeGFPLuc complexes that were constructed at MNP-to-virus ratios of 10 fg Fe/VP at varying low doses of infectious virus particles per cell (MOI) under a magnetic field. After 72 h of incubation, luciferase reporter expression was analyzed in cell lysates. SO-Mag6-*n* particles were obtained by the attachment of PEI to silica-oxide SO-Mag5 MNPs at different PEI-to-iron *w/w* % ratios *n*.

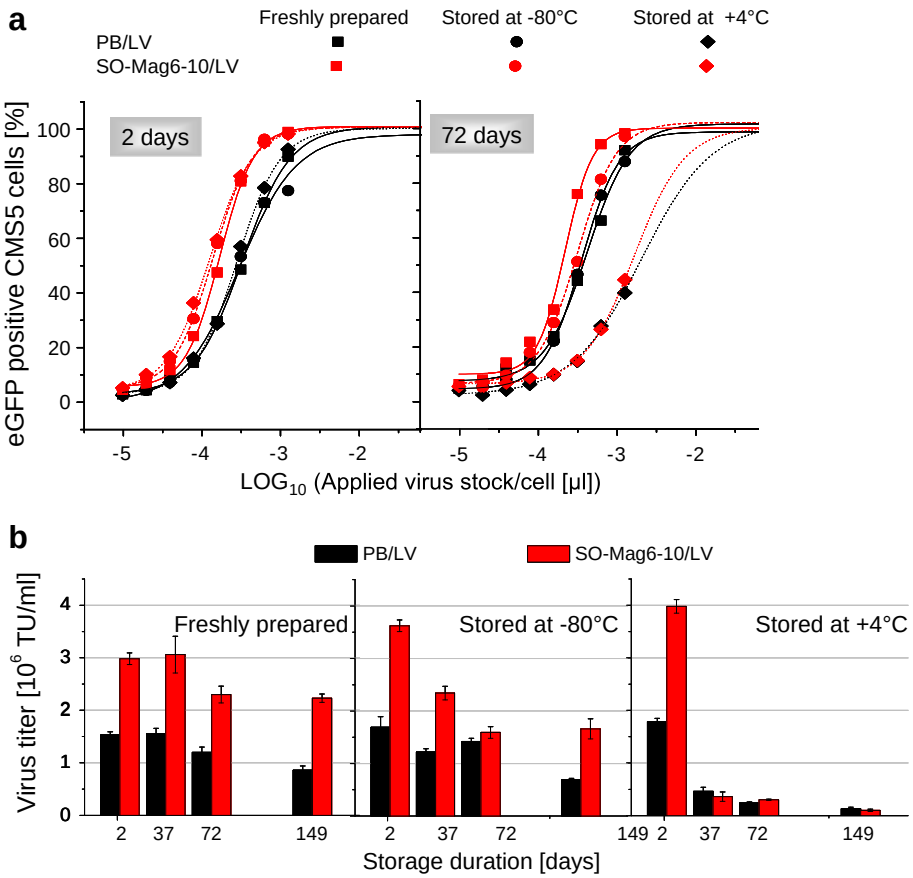

Fig. 7 Time course of the infectivity of the lentiviral vectors during storage in complexes with silica iron oxide MNPs decorated with PEI. Complexes of the lentiviral vector LVSFeGFP with either SO-Mag6-10 MNPs that was constructed at 10 fg Fe/VP (SO-Mag6-10/LV) or polybrene (PB/LV) were (i) freshly prepared and stored at (ii) −80°C or (iii) +4°C. After 2, 37, 72 or 149 days of storage, CMS5 cells were infected with different doses of the complexes or with freshly prepared complexes, and no magnetic field was applied. After 48 h of cultivation, the percentage of eGFP-positive cells was determined by FACS analysis and plotted against the applied volume of the virus stock per cell as shown in Figure **a** for infections that were performed after 2 days and 72 days of storage. (**b**) Virus titers were derived from the stock volumes resulting in 50% eGFP-expressing cells as determined after the fitting of the dose-effect curves with a logistic function. SO-Mag6-10 particles were obtained by the association of PEI to silica-oxide SO-Mag5 MNPs at a PEI-to-iron *w/w* % ratio of 10.

magnetic field that has previously been established for the magnetic vectors of the oncolytic adenovirus Ad520 (15,41).

Importantly, the magnetic complexes also showed higher transduction efficiencies than those of the polybrene-supported complexes at different time points during the 5-month storage. It is also noteworthy that after 2 days of storage at +4°C, no deactivation was observed for either the polybrene or magnetic complexes. This stability of the complexes over the course of storage could prove to be favorable in further potential applications.

Cell Association and Cytotoxicity of Silica-Iron Oxide Nanoparticles Decorated with Polyethylene Imine

Cell association/internalization and cytotoxicity (based on the MTT-test respiration activity assay) were evaluated in SHSY5Y human neuroblastoma cells (Fig. 8). The primary SO-Mag5 particles are not readily internalized, and loading with 1 w% PEI increased the cell association and internalization of the particles, whereas with PEI loading levels of 3–12%, they were very readily internalized and showed high labeling efficiencies (Fig. 8a). The respiration rates of the neuroblasts remained higher than 75% of the reference values for the untreated cells when up to 12 pg of iron were loaded per cell. For the viral complexes that were constructed with 10 fg Fe/VP, which was found to be an optimum MNP-to-virus ratio for numerous transduction experiments, the 12 pg of applied iron per cell would correspond to an applied virus dose of 1200 physical virus particles per cell. This virus dose was found to be high enough to enable a high magnetotransduction efficiency using both lentiviral and adenoviral gene delivery vectors (15,26,41).

The data on the cell respiration rates plotted against internalized/associated iron (derived from the data shown in Fig. 8a) show that the effects of the nanoparticles depend

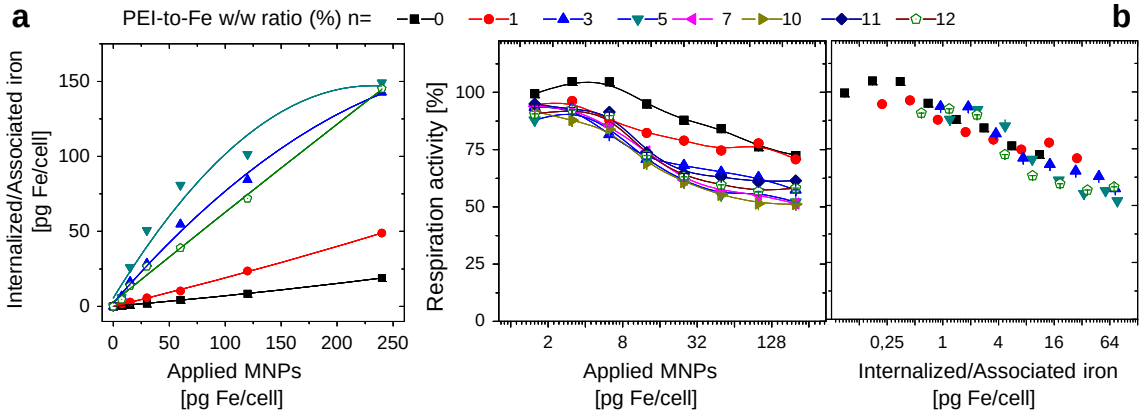

Fig. 8 Cell association and effect on cell viability of silica-iron oxide nanoparticles decorated with polyethylenimine. The SHSY5Y human neuroblasts were incubated with silica-iron oxide SO-Mag5 particles and that were titrated with PEI at different PEI-to-iron *w/w* % ratios *n* as indicated in the figure. (**a**) After 24 h of incubation, particle association/internalization into cell was determined by measuring the cell-associated non-heme iron concentration. (**b**) 48 h after the loading of the magnetic nanoparticles, the respiration activity of the cells was measured by the MTT assay and plotted against applied (left panel) or internalized/associated (right panel) iron doses derived from the data shown in (**a**). Each value represents the mean ± SD ($n = 3$).

solely on the dose of the internalized iron, which is similar for the primary particles and those loaded with 12w% PEI (plot at the right panel of Fig. 8b). Thus, the surface structures of the particles have more effects on their interactions with cell membranes and their capacities for internalization than on the toxicities of the internalized particles.

During the cell labeling procedure, the particles were administered to the cells in the cell culture medium. The electrokinetic potential of the particles that were diluted with the cell culture medium containing 10% FCS were nearly neutral or negative (approximately −10 mV) for all of the particles tested, including the primary SO-Mag5 particles (negatively charged in the water suspension) and all of the particles that were decorated with PEI (positively charged in the water suspension) (see data in Fig. 3a (DMEM + 10% FCS)). Apparently, the adsorption of the ions and association with the proteins from the cell culture medium induce a net surface charge reversal. There was no correlation observed between cell labeling efficiencies and surface charges or the sizes of the particle assemblies (D_h).

Evaluation of MRI Contrast Efficiency of Free and Cell-Associated MNPs

Non-invasive quantification of MNP-facilitated gene or viral delivery is of interest for *in vivo* drug efficacy studies. To evaluate the MRI contrast effects (relaxivities) of the primary silica-iron oxide nanoparticles and the particles that were decorated with PEI and to quantify the effects of the cellular internalization on the relaxivities, we performed imaging experiments on a clinical 1.5 T MRI system. The 2 to 3 dilutions of the particles and the cells labeled with the SO-Mag6-11.5 particles were homogenously distributed in agarose gel phantoms that were doped with nickel (II) ions (44) to adjust the relaxation rates to the baseline tissue parameters of either rat liver or mouse pancreatic ductal adenocarcinoma (PDAC) tissues as described in detail in the Material and Methods.

The resulting T_2^* ME-FFE and R_2^* mapping data for the SO-Mag5 MNPs that are homogeneously distributed in the rat liver-mimicking phantom are shown in Fig. 9a. Both the R_2 and the R_2^* relaxation rates linearly increase with increasing iron concentrations in the range of 0.2–24 μg Fe/ml of free and cellular-associated MNPs. Interestingly, primary silica iron oxide nanoparticles possess high r_2 relaxivity of 435±10 (s^{-1} (mM Fe)$^{-1}$) compared to the SO-Mag6-11.5 particles that are decorated with PEI (only 32.1±0.8 s^{-1} (mM Fe)$^{-1}$) in the same liver tissue-mimicking phantom (Table I). Similar effects of the surface coatings were observed by Zhang *et al.* (53); the highest transverse relaxivity of r_2=39.80±0.22 s^{-1} mM^{-1} was achieved for the silica coated USPIO particles with a core size of approximately 10 nm, whereas the particles with similar core sizes that were stabilized by the hydrolization and condensation of (3-aminopropyl)trimethoxysilane and [*N*-(2-aminoethyl)-3-aminopropyl]trimethoxysilane reached T_2 relaxivities of only 134.40±0.01 and 84.79±0.02 s^{-1} mM^{-1}, respectively (53).

The plotting and fitting of the mean R_2^* of the wells over the respective iron concentrations (Fig. 9c) yielded very high transverse relaxivities of both the primary and PEI-modified silica iron oxide particles. The SO-Mag5 MNPs exhibited a relaxivity of r_2^*=697±13 s^{-1} (mM Fe)$^{-1}$. The r_2^* values that were measured for the SO-Mag6-11.5 nanoparticles that were distributed in the rat liver tissue and mPDAC tissue-mimicking phantoms were 837±8 s^{-1} (mM Fe)$^{-1}$ and 767±12 s^{-1} (mM Fe)$^{-1}$, respectively.

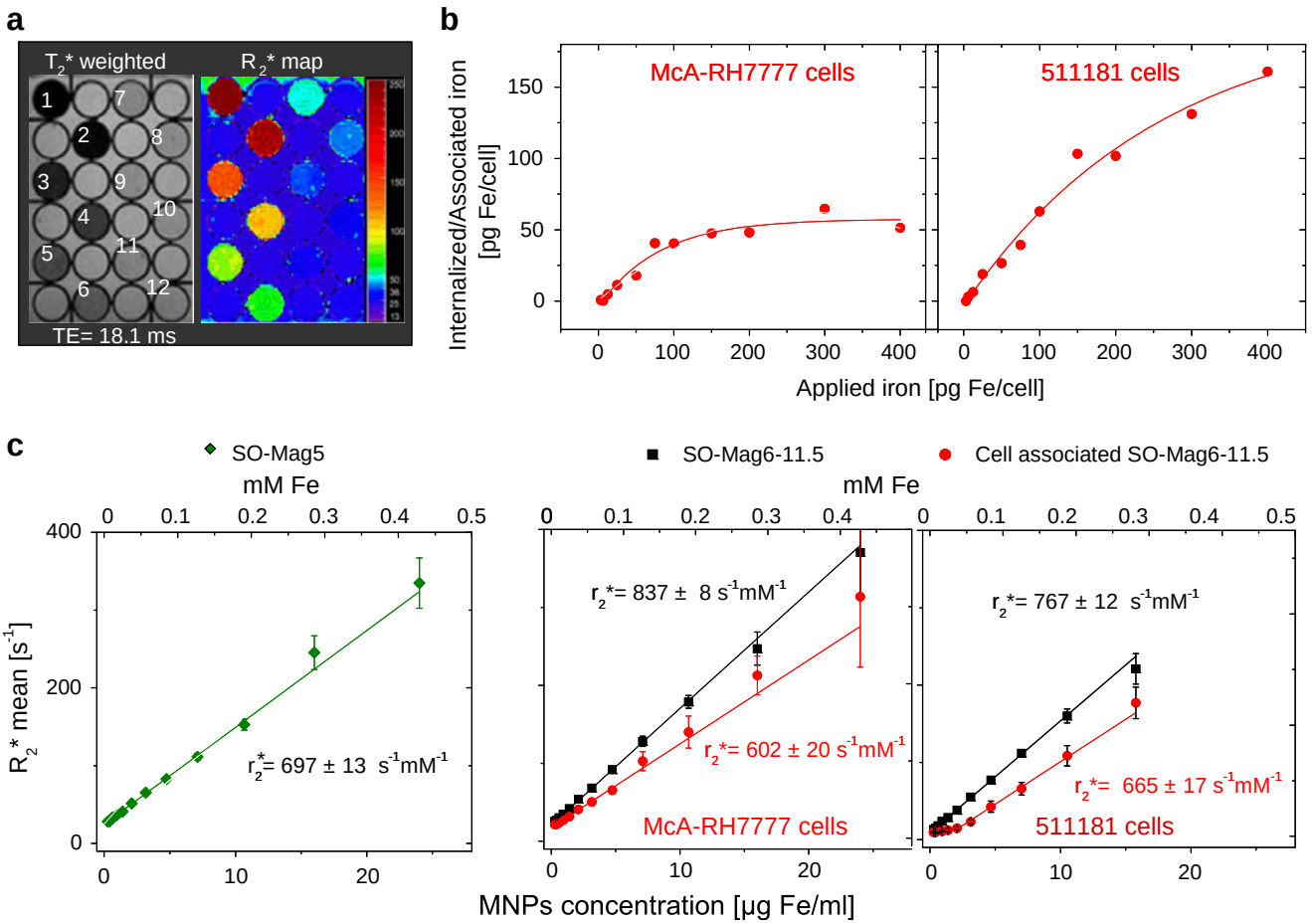

Fig. 9 MRI contrast efficiency of the silica iron oxide MNPs. (**a**) MRI calibration of MNPs. The magnitude image (echo time *TE*=18.1 ms) of the T_2^*, a multi-echo gradient echo sequence (FFE) (left), and the corresponding color-coded R_2^* [s^{-1}] map (right) showing the SO-Mag5 nanoparticle calibration phantom with the particles homogeneously distributed in the agarose gel, mimicking mouse liver tissue relaxivity. Only the numbered wells contain the MNPs. The remainder of the wells and the spaces between the wells contain agarose gel only. The highest MNP concentration (in well number 1) is 24 µg Fe/ml. Subsequent wells (2 to 12) contain decreasing concentrations from a 2 to 3 dilution series of the MNPs. (**b**) Labeling of the McA-RH7777 rat hepatocellular carcinoma and mouse pancreatic ductal adenocarcinoma or 511181 cells with the SO-Mag6-11.5 nanoparticles. The iron concentration per cell for the internalized/associated MNPs *versus* the applied iron doses per cell according to the chemical analysis of non-heme iron. (**c**) The dependency of the mean ± SD R_2^* from MNP or the iron concentrations in the wells and the resulting linear fit showing the calculated transverse relaxivity (r_2^*) values for the SO-Mag6-11.5 MNPs and the MNPs associated with the homogeneously distributed cells in the calibration that were phantoms mimicking the relaxivities of rat liver (McA-RH7777 cells were loaded with 39 pg Fe/cell) and mouse pancreatic ductal adenocarcinoma (511181 cells were loaded with 28 pg Fe/cell) tissues, respectively. The phantom with the SO-Mag5 MNPs that was prepared with the mouse liver tissue-mimicking gel also showed 24 µg Fe/ml as its highest iron concentration.

The appropriate conditions for cell loading with the MNPs were chosen based on the results of the MNP cell labeling experiments that are shown in Fig. 9b. To prepare the rat liver and mPDAC phantoms, McA-RH7777 and 511181 cells were loaded with 39 and 28 pg Fe/cell, and the maximal cell concentration was 6.2×10^5 cells ml^{-1} and 8.6×10^5 cells ml^{-1}, respectively.

Mean R_2^* values that were measured in calibration phantoms of homogenous distributions of MNP-labeled cells plotted against the iron concentrations are given in Fig. 9c. Cell concentrations as low as 1.4 µg Fe/ml (at least 39,000 cells/ml and approximately 50,000 cells/ml at cell iron loading levels of 39 pg Fe/cell and 28 pg Fe/cell, respectively) were detectable.

The r_2^* relaxivities of SO-Mag6-11.5 were 15-20-fold and 20-40-fold higher than the r_2 values in the rat liver and mPDAC tissue-mimicking phantoms, respectively (Table I). Cell association decreased the r_2 relaxivities of the MNPs by 42 to 55%, whereas r_2^* relaxivity was only 13 to 28% lower for the cell-associated MNPs compared to that of the free, homogeneously distributed particles. These observations were in agreement with previous reports that described that R_2^*-weighted acquisitions are likely to be the most sensitive to the presence of iron-oxide particles (54,55). The modulation of the intracellular relaxivities of the MNPs resulting presumably from the intracellular "clusterization" of the internalized particles has been previously described;

Table I r_2 and r_2* Relaxivities (s^{-1} (mM Fe)$^{-1}$) for Free and Cell-Associated MNPs in Agarose-Ni(II) Tissue-Mimicking Phantoms Determined Using Clinical 1.5 T MRI System

	Liver tissue-mimicking phantom[a]			Pancreatic ductal adenocarcinoma tissue-mimicking phantom[b]		
	r_2	r_2*	r_2*/ r_2	r_2	r_2*	r_2*/ r_2
SO-Mag5	435 ± 10	697 ± 13	1.6	–	–	–
SO-Mag6-11.5	54.9 ± 1.7	837 ± 8	15.2	37.4 ± 0.7	767 ± 12	20.5
Cell-associated SO-Mag6-11.5	McA-RH7777 hepatocellular carcinoma cells			Mouse pancreatic ductal adenocarcinoma cells		
	32.1 ± 0.8	602 ± 20	18.8	16.8 ± 1.1	665 ± 17	39.6
Reduction of MNP relaxivities (%) by cell association	42	28	–	55	13	–

[a] Basal (0 μg Fe/ml) R_2 (s^{-1}) = 12.9 ± 0.2 and R_2*(s^{-1}) = 21.0 ± 0.6;
[b] Basal R_2 (s^{-1}) = 5.0 ± 0.1 and R_2*(s^{-1}) = 11.0 ± 1.4

both increases and decreases in the r_2 relaxivities of the cell-associated iron were observed compared to the free particles, depending on the particle type, their surface properties and the cell type (55–57). The clustering of nanoparticles and their magnetism was also shown to be dependent on the targeted organ, on the dose administrated and on the time elapsed since their injection (58). How long can the cells be imaged by MRI depends on the dilution of the particles by either cell proliferation or cell death followed by macrophage uptake, and is different for cells with high and low mitotic activity (59). Biotransformation or biodegradation of the particles and related evolution of their magnetic properties (58) is another factor that affects the relaxivities and MRI detection limit.

The r_2* relaxivity characteristics of both the primary and PEI-modified silica iron oxide nanoparticles that are described in our study make them promising agents for the *in vivo* MRI imaging of magnetic gene delivery vector constructions and cell-tracking experiments.

DISCUSSION

In a search for efficient formulations for viral and non-viral nucleic acid delivery while minimizing toxicity a lot PEI/iron oxide systems were described starting from the first magnetic iron oxide nanoparticles stabilized with high molecular 800 kD PEI (CombiMag, Chemicell) (4), followed by PolyMag (Chemicell) and numerous particles with coatings containing different molecular weight PEIs, combined with other polymers and/or surfactants (6–11). We and other have learned that there is no one "magic" type of nanoparticles universally applicable with all vectors and cell types (1). We have tested magnetic lipoplexes and polyplexes with different domestic synthesized MNPs and commercially available CombiMag and PolyMag nanoparticles in terms of transfection efficiency in suspended human Jurkat T cells and determined the cytotoxicity of magnetic vectors (16). PolyMag-plasmid DNA complexes showed low transfection efficiency and high toxicity. Lipoplexes with palmitoyl dextran modified MNPs as well as lipoplexes with PEI-Mag2 nanoparticles coated with self-assembling layers of fluorinated surfactant FSA combined with PEI demonstrated about 2-fold higher transfection efficiency in Jurkat T cells in terms of the percentage of transfected cells compared to CombiMag lipoplexes. Further screening has shown that lentiviral complexes formulated at 10 fg Fe/VP with silica iron oxide MNPs decorated with 5w% PEI (SO-Mag2) were about 2 times and 2.5 times more efficient than complexes of PEI-Mag2 and ViroMag R/L (OZ BioSciences) MNPs, respectively, in transduction of 3T3 NIH mouse fibroblasts; there was no additional toxicity associated with the particles within the tested concentration range, as compared to the non-magnetic lipoplexes, except for the highly toxic PolyMag complexes (60). SO-Mag2 lipoplexes yielded also highest percentage of transfected Jurkat T cells after non-viral magselectofection (60). The uptake of magnetic complexes into cells was quantified using radioactive labelled DNA in order to determine whether uptake alone accounts for transfection efficiency. No significant differences in uptake were found for the three tested magnetic complexes. Hence, uptake alone does not account for the observed differences. Further usage of these silica-iron oxide nanoparticles decorated with 5w% PEI for non-viral and viral magselectofection resulted in a considerable enhancement of transfection/transduction efficiency in Jurkat T cells, hematopoietic and mesenchymal stem cells (26). Assembling of these particles with oncolytic adenovirus confers high protection against inhibitory effects of high serum concentration and neutralizing antibody while enhancing the oncolytic productivity of the internalized virus (15). Another advantage of viral and non-viral complexes with these nanoparticles is their high magnetic responsiveness (15,26,60) that could contribute to the high efficacy observed *in vivo* (15).

In this work, we aimed at finding a formulation for silica-iron oxide MNPs decorated with 25-kD branched PEIs that is stable in aqueous suspensions, associates with viral particles into stable complexes in the presence of high serum concentrations and allows for efficient magnetotransduction *in vitro*. We have specifically looked at the association of PEI loading with the satisfactory characteristics of each of the optimization parameters (Fig. 10).

To synthesize the core material of the nanoparticles, we have used a simple method for iron hydroxide precipitation from an aqueous solution of Fe(II)/Fe(III) salts, which we have described previously. The silica coating at the surface of freshly formed iron oxide nanocrystals was obtained by hydrolysis and the condensation of TEOS. Following the results of Bagwe *et al.* (61), who systematically searched for the means to reduce aggregation of functionalized silica nanoparticles, we have used THPMP organosilane to introduce phosphonate groups onto the surface of the silica coating to reduce aggregation and improve the colloidal stability of the particles. Ammoniac served both to precipitate the iron hydroxide and to act as a catalyst for hydrolysis of the tetraethyl orthosilicate and organosilane. This approach resulted in SO-Mag5 nanoparticles with average core sizes of approximately 7 nm and high saturation magnetization levels of 94 emu/g Fe that possessed on average 8.4 phosphonate groups per nm^2 of surface coating, ensuring for the highly negative electrokinetic potential of the particles (-38.0 ± 2.0 mV) in aqueous suspensions, which enabled the association of the PEI by electrostatic interaction.

Increasing the PEI loading shifted the electrokinetic potential from a highly negative to a highly positive state with a charge reversal and a stationary value of approximately +40 mV at a PEI-to-iron *w*/*w* ratio of above 5%.

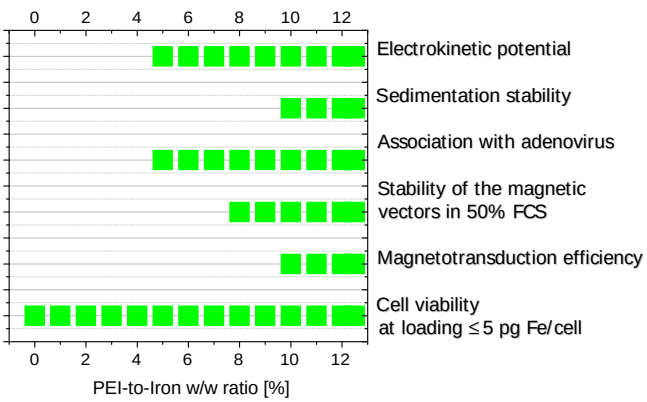

Fig. 10 Summary of optimization results. The green bars outline the ranges of the PEI-to-iron *w*/*w* % ratios for the silica-iron-oxide SO-Mag5 particles decorated with PEI that were the most concordant with each of the optimization parameters for efficient gene delivery.

The time- and space-resolved detection of light transmission (STEP-technology) combined with analytical centrifugation revealed information on the colloidal stability and particle size distributions of the MNP suspensions in the PEI loading range of >5%, at which no more changes in the electrokinetic potential occurred. At the lowest PEI concentrations (1–3%), the dispersion was completely flocculated. For PEI loadings exceeding 5% of the iron mass, a subfraction of non-flocculated particles appeared whose ratios increased gradually until the particles were completely dispersed at 10–12% PEI. Accounting for the MNP particle average weight of 6.2×10^{-19} g Fe, 12% PEI corresponds to 7.4×10^{-20} g/particle or 1.8 PEI molecules /particle.

Particles that were loaded with more than 5% PEI are suitable for quantitative association and magnetic sedimentation with the adenovirus at iron-to-virus ratios of 5–20 fg iron per virus particle. However, high PEI levels (PEI-to-iron *w*/*w* ratio ≥7%) were necessary to ensure the sufficient stability (for at least 30 min) of the magnetic vector in 50% FCS. With a lentiviral vector, the maximum transduction efficiency was achieved for the particles with 10–12% PEI loading. The lentiviral complexes with the nanoparticles decorated with 10% PEI can be stored frozen without any loss of virus infectivity compared to the naked virus.

In contrast to the primary SO-Mag5, PEI coated particles display high cell labeling efficiencies. All examined particles having positive charge in the aqueous suspension, have a net neutral or negative charge in the cell culture medium. We have not observed any correlation between the net charges or sizes of the particles in the cell culture medium and the cell labeling efficiencies. There is an abundance of data available that highlight the roles of size and surface properties, such as charge and hydrophylicity, on efficiency of cell labeling with magnetic nanoparticles. Both positively and negatively charged particles can be efficiently internalized (56,62). Polycations are known to facilitate particle binding to the anionic cell membrane and increase uptake (63). One can speculate that despite the net neutral or negative charges of the particle assemblies in the cell culture medium, the local nanoscale charge inhomogenities can enable association with the cell membrane (64–66). Similar mechanisms are used to assemble the particles at nanoscale charge patterns generated at template surfaces (67). In our case, local charge inhomogenities originate from negatively charged phosphonate groups and positively charged PEI chains on the surface layers of the particles.

Primary silica iron oxide SO-Mag5 nanoparticles had high r_2 relaxivities of 435 ± 10 (s^{-1} (mM Fe)$^{-1}$). Both the SO-Mag5 particles and those that were loaded with optimal amounts of PEI to allow for the stability and high transduction efficiencies of the magnetic vectors showed excellent r_2* relaxivities (higher than 600 s^{-1} (mM Fe)$^{-1}$) for the free and cell-internalized particles, suggesting the utility of MRI

imaging in the assessment of MNP-loaded cells *in vivo*. The high saturation magnetization of the core materials (94 emu/g Fe) and a thick stabilizing coating of the silica iron oxide particles can both contribute to the high r_2* transverse relaxivities of the developed nanomaterials (68,69).

CONCLUSION

The results of this study show that the attachment of PEI to the designed silica-iron oxide nanoparticles with PEI-to-iron *w*/*w* ratios of 10–12% allows for high colloidal stability and the efficient association with viral vectors into optimized magnetic viral complexes being stable In the presence of high protein concentrations and enabling highly efficient magnetotransduction *in vitro* without causing cell toxicity. The high r_2* relaxivities of the materials are suggestive of the MRI imaging modality.

ACKNOWLEDGMENTS & DISCLOSURES

We greatly appreciate the help of Edelburga Hammerschmid with the flow cytometry analysis and thank Dr. Uwe Vohrer and Dr. Joachim Mayer from the Fraunhofer Institute for Interfacial Engineering and Biotechnology IGB for the XPS analysis of the nanomaterials. We also thank Dr. Elena Oranskaya from the Ukrainian Academy of Sciences for her help with the X-ray diffraction. Financial support from the German Research Foundation through the DFG Research Unit FOR917 (Projects PL 281/3-1, TR 408/6-1 and AN 333/1-1) and the German Excellence Cluster m^4 entitled "Nanosystems Initiative Munich", the German Federal Ministry of Education (Project ELA 10/002) and the German Federal Ministry of Economics (Project 0327414C, LUM) are gratefully acknowledged.

Prof. Dr. Christian Plank is a co-founder of OZ Biosciences, SA, Marseille France. OZ Biosciences commercializes reagents for magnetofection. Prof. Dr. Dietmar Lerche is a managing director of LUM Gesellschaft für Labor-, Umweltdiagnostik & Medizintechnik m.b.H. LUM GmbH develops, produces and commercializes analytical devices for dispersion analysis and particle characterization.

REFERENCES

1. Plank C, Zelphati O, Mykhaylyk O. Magnetically enhanced nucleic acid delivery. Ten years of magnetofection-Progress and prospects. Adv Drug Deliv Rev. 2011; 63:1300–31.
2. Hughes C, Galea-Lauri J, Farzaneh F, Darling D. Streptavidin paramagnetic particles provide a choice of three affinity-based capture and magnetic concentration strategies for retroviral vectors. Mol Ther. 2001;3:623–30.
3. Mah C, Fraites JTJ, Zolotukhin I, Song S, Flotte TR, Dobson J, Batich C, Byrne BJ. Improved method of recombinant AAV2 delivery for systemic targeted gene therapy. Mol Ther. 2002;6:106–12.
4. Scherer F, Anton M, Schillinger U, Henke J, Bergemann C, Kruger A, Gansbacher B, Plank C. Magnetofection: enhancing and targeting gene delivery by magnetic force *in vitro* and *in vivo*. Gene Ther. 2002;9:102–9.
5. Chorny M, Fishbein I, Alferiev I, Levy RJ. Magnetically responsive biodegradable nanoparticles enhance adenoviral gene transfer in cultured smooth muscle and endothelial cells. Mol Pharm. 2009;6:1380–7.
6. Hofmann A, Wenzel D, Becher UM, Freitag DF, Klein AM, Eberbeck D, Schulte M, Zimmermann K, Bergemann C, Gleich B, Roell W, Weyh T, Trahms L, Nickenig G, Fleischmann BK, Pfeifer A. Combined targeting of lentiviral vectors and positioning of transduced cells by magnetic nanoparticles. Proc Natl Acad Sci U S A. 2009;106:44–9.
7. Shi Y, Zhou L, Wang R, Pang Y, Xiao W, Li H, Su Y, Wang X, Zhu B, Zhu X, Yan D, Gu H. *In situ* preparation of magnetic nonviral gene vectors and magnetofection *in vitro*. Nanotechnology. 2010;21:115103.
8. Namgung R, Singha K, Yu MK, Jon S, Kim YS, Ahn Y, Park IK, Kim WJ. Hybrid superparamagnetic iron oxide nanoparticle-branched polyethylenimine magnetoplexes for gene transfection of vascular endothelial cells. Biomaterials. 2010;31:4204–13.
9. Brunot C, Ponsonnet L, Lagneau C, Farge P, Picart C, Grosgogeat B. Cytotoxicity of polyethyleneimine (PEI), precursor base layer of polyelectrolyte multilayer films. Biomaterials. 2007;28:632–40.
10. Ang D, Nguyen QV, Kayal S, Preiser PR, Rawat RS, Ramanujana RV. Insights into the mechanism of magnetic particle assisted gene delivery. Acta Biomater. 2011;7:1319–26.
11. Nguyen HK, Lemieux P, Vinogradov SV, Gebhart CL, Guerin N, Paradis G, Bronich TK, Alakhov VY, Kabanov AV. Evaluation of polyether-polyethyleneimine graft copolymers as gene transfer agents. Gene Ther. 2000;7:126–38.
12. Kami D, Takeda S, Itakura Y, Gojo S, Watanabe M, Toyoda M. Application of magnetic nanoparticles to gene delivery. Int J Mol Sci. 2011;12:3705–22.
13. Arsianti M, Lim M, Marquis CP, Amal R. Polyethylenimine based magnetic iron-oxide vector: the effect of vector component assembly on cellular entry mechanism, intracellular localization, and cellular viability. Biomacromolecules. 2010;11:2521–31.
14. Arsianti M, Lim M, Marquis CP, Amal R. Assembly of polyethylenimine-based magnetic iron oxide vectors: insights into gene delivery. Langmuir. 2010;26:7314–26.
15. Tresilwised N, Pithayanukul P, Holm PS, Schillinger U, Plank C, Mykhaylyk O. Effects of nanoparticle coatings on the activity of oncolytic adenovirus-magnetic nanoparticle complexes. Biomaterials. 2012;33:256–69.
16. Sanchez-Antequera Y, Mykhaylyk O, Thalhammer S, Plank C. Gene delivery to Jurkat T cells using non-viral vectors associated with magnetic nanoparticles. Int J Biomed Nanoscience Nanotechnology. 2010;1:202–29.
17. Pasqua L, Cundari S, Ceresa C, Cavaletti G. Recent development, applications, and perspectives of mesoporous silica particles in medicine and biotechnology. Curr Med Chem. 2009;16:3054–63.
18. Vivero-Escoto JL, Slowing II, Trewyn BG, Lin VS. Mesoporous silica nanoparticles for intracellular controlled drug delivery. Small. 2010;6:1952–67.
19. Stober W, Fink A, Bohn E. Controlled growth of monodisperse silica spheres in micron size range. J Colloid Interface Sci. 1968;26:62–9.

20. Vogt C, Toprak MS, Muhammed M, Laurent S, Bridot JL, Muller RN. High quality and tuneable silica shell-magnetic core nanoparticles. J Nanoparticle Res. 2010;12:1137–47.
21. Selvan ST, Tan TT, Ying JY. Robust, non-cytotoxic, silica-coated CdSe quantum dots with efficient photoluminescence. Adv Mater. 2005;17:1620.
22. Sotiriou GA, Hirt AM, Lozach PY, Teleki A, Krumeich F, Pratsinis SE. Hybrid, silica-coated, janus-like plasmonic-magnetic nanoparticles. Chem Mater. 2011;23:1985–92.
23. Wiesner U, Suteewong T, Sai H, Lee J, Bradbury M, Hyeon T, Gruner SM. Ordered mesoporous silica nanoparticles with and without embedded iron oxide nanoparticles: structure evolution during synthesis. J Mater Chem. 2010;20:7807–14.
24. Yiu HHP, McBain SC, Lethbridge ZAD, Lees MR, Dobson J. Preparation and characterization of polyethylenimine-coated Fe3O4-MCM-48 nanocomposite particles as a novel agent for magnet-assisted transfection. J Biomed Mater Res Part A. 2010;92A:386–92.
25. Mykhaylyk O, Sanchez-Antequera Y, Vlaskou D, Hammerschmid E, Anton M, Zelphati O, Plank C. Liposomal magnetofection. Meth Mol Biol. 2010;605:487–525.
26. Sanchez-Antequera Y, Mykhaylyk O, van Til NP, Cengizeroglu A, de Jong JH, Huston MW, Anton M, Johnston ICD, Pojda Z, Wagemaker G, Plank C. Magselectofection: an integrated method of nanomagnetic separation and genetic modification of target cells. Blood. 2011;117:E171–81.
27. Cebrián V, Yagüe C, Arruebo M, Martín-Saavedra F, Santamaría J, Vilaboa N. On the role of the colloidal stability of mesoporous silica nanoparticles as gene delivery vectors. J Nanoparticle Res. 2011;1–12.
28. Bringley JF, Wunder A, Howe AM, Wesley RD, Qiao TA, Liebert NB, Kelley B, Minter J, Antalek B, Hewitt JM. Controlled, simultaneous assembly of polyethylenimine onto nanoparticle silica colloids. Langmuir. 2006;22:4198–207.
29. Mykhaylyk O, Antequera YS, Vlaskou D, Plank C. Generation of magnetic nonviral gene transfer agents and magnetofection in vitro. Nat Protoc. 2007;2:2391–411.
30. Matz H, Drung D, Hartwig S, Gross H, Kotitz R, Muller W, Vass A, Weitschies W, Trahms L. A SQUID measurement system for immunoassays. Appl Supercond. 1998;6:577–83.
31. Eberbeck D, Wiekhorst F, Steinhoff U, Trahms L. Aggregation behaviour of magnetic nanoparticle suspensions investigated by magnetorelaxometry. J Phys Condens Matter. 2006;18:S2829–46.
32. Eberbeckand D, Trahms L. Experimental investigation of dipolar interaction in suspensions of magnetic nanoparticles. J Magn Magn Mater. 2011;323:1228–32.
33. Badolato GG, Aguilar F, Schuchmann HP, Sobisch T, Lerche D. Evaluation of long term stability of model emulsions by multisample analytical centrifugation. Surf Interfacial Forces Fund Appl. 2008;134:66–73.
34. Sobischand T, Lerche D. Thickener performance traced by multisample analytical centrifugation. Colloid Surface Physicochem Eng Aspect. 2008;331:114–8.
35. Detloff T, Sobisch T, Lerche D. Particle size distribution by space or time dependent extinction profiles obtained by analytical centrifugation (concentrated systems). Powder Technol. 2007;174:50–5.
36. Wübbenhorst D, Dumler K, Wagner B, Wexel G, Imhoff A, Gansbacher B, Vogt S, Anton M. Tetracycline-regulated bone morphogenetic protein 2 gene expression in lentivirally transduced primary rabbit chondrocytes for treatment of cartilage defects. Arthritis Rheum. 2010;62:2037–46.
37. Barry SC, Harder B, Brzezinski M, Flint LY, Seppen J, Osborne WRA. Lentivirus vectors encoding both central polypurine tract and posttranscriptional regulatory element provide enhanced transduction and transgene expression. Hum Gene Ther. 2001;12:1103–8.
38. Herenu CB, Sonntag WE, Morel GR, Portiansky EL, Goya RG. The ependymal route for insulin-like growth factor-1 gene therapy in the brain. Neuroscience. 2009;163:442–7.
39. Hitt M, Bett AJ, Addison CL, Prevec L, Graham FL. Techniques for human adenovirus vector construction and characterization. In: KW A, editor. Viral gene techniques. San Diego, New York, Boston, London, Sydney, Tokyo, Toronto: Academic; 1995. p. 13–30.
40. Mittereder N, March KL, Trapnell BC. Evaluation of the concentration and bioactivity of adenovirus vectors for gene therapy. J Virol. 1996;70:7498–509.
41. Tresilwised N, Pithayanukul P, Mykhaylyk O, Holm PS, Holzmuller R, Anton M, Thalhammer S, Adiguzel D, Doblinger M, Plank C. Boosting oncolytic adenovirus potency with magnetic nanoparticles and magnetic force. Mol Pharm. 2010;7:1069–89.
42. Mykhaylyk O, Steingotter A, Perea H, Aigner J, Botnar R, Plank C. Nucleic acid delivery to magnetically-labeled cells in a 2D array and at the luminal surface of cell culture tube and their detection by MRI. J Biomed Nanotechnol. 2009;5:692–706.
43. Berridge MV, Herst PM, Tan AS. Tetrazolium dyes as tools in cell biology: new insights into their cellular reduction. Biotechnol Annu Rev. 2005;11:127–52.
44. Christoffersson JO, Olsson LE, Sjoberg S. Nickel-doped agarose-gel phantoms in Mr imaging. Acta Radiologica. 1991;32:426–31.
45. Dahnke H, Schaeffter T. Limits of detection of SPIO at 3.0 T using T2* relaxometry. Magn Reson Med. 2005;53:1202–6.
46. Ogradyand K, Bradbury A. Particle-size analysis in ferrofluids. J Magn Magn Mater. 1983;39:91–4.
47. Hunt CP, Moskowitz BM, Banerjee SK. Magnetic properties of rocks and minerals. Rock Physics and Phase Relations: A Handbook of Physical Constants, American Geophysical Union, Washington D.C., 1995, p. 189.
48. Lu AH, Salabas EL, Schuth F. Magnetic nanoparticles: synthesis, protection, functionalization, and application. Angew Chem Int Ed. 2007;46:1222–44.
49. Göpel W. "Magnetic dead layers" on chemisorption at ferromagnetic surfaces. Surf Sci. 1979;85:400–12.
50. Shendrukand TN, *et al.* The effect of surface spin disorder on the magnetism of Î³-Fe_2O_3 nanoparticle dispersions. Nanotechnology. 2007;18:455704.
51. Goya GF, Berquo TS, Fonseca FC, Morales MP. Static and dynamic magnetic properties of spherical magnetite nanoparticles. J Appl Phys. 2003;94:3520–8.
52. Anton M, Wolf A, Mykhaylyk O, Koch C, Gansbacher B, Plank C. Optimising Adenoviral Transduction of endothelial cells under flow. Pharm Res. 2011. doi:10.1007/s11095-011-0631-2.
53. Zhang C, Wängler B, Morgenstern B, Zentgraf H, Eisenhut M, Untenecker H, Krüger R, Huss R, Seliger C, Semmler W, Kiessling F. Silica- and alkoxysilane-coated ultrasmall superparamagnetic iron oxide particles: a promising tool to label cells for magnetic resonance imaging. Langmuir. 2007;23:1427–34.
54. Bowen CV, Zhang X, Saab G, Gareau PJ, Rutt BK. Application of the static dephasing regime theory to superparamagnetic iron-oxide loaded cells. Magn Reson Med. 2002;48:52–61.
55. Kuhlpeter R, Dahnke H, Matuszewski L, Persigehl T, von Wallbrunn A, Allkemper T, Heindel WL, Schaeffter T, Bremer C. R2 and R2* mapping for sensing cell-bound superparamagnetic nanoparticles: in vitro and murine *in vivo* testing1. Radiology. 2007;245:449–57.
56. Billotey C, Wilhelm C, Devaud M, Bacri JC, Bittoun J, Gazeau F. Cell internalization of anionic maghemite nanoparticles: quantitative effect on magnetic resonance imaging. Magn Reson Med. 2003;49:646–54.
57. Klug G, Kampf T, Bloemer S, Bremicker J, Ziener CH, Heymer A, Gbureck U, Rommel E, Nöth U, Schenk WA, Jakob PM, Bauer WR. Intracellular and extracellular T1 and T2 relaxivities of magneto-optical nanoparticles at experimental high fields. Magn Reson Med. 2010;64:1607–15.

58. Levy M, Wilhelm C, Luciani N, Deveaux V, Gendron F, Luciani A, Devaud M, Gazeau F. Nanomagnetism reveals the intracellular clustering of iron oxide nanoparticles in the organism. Nanoscale. 2011;3:4402–10.
59. Rogers WJ, Meyer CH, Kramer CM. Technology Insight: *in vivo* cell tracking by use of MRI. Nat Clin Pract Cardiovasc Med. 2006;3:554–62.
60. Sánchez Antequera Y. Magselectofection: A novel integrated technology of magnetic separation and genetic modification of target cells Fakultät für Chemie und Pharmazie Vol. Dr., LMU München, München, 2010, pp. 136, http://edoc.ub.uni-muenchen.de/12746/.
61. Bagwe RP, Hilliard LR, Tan WH. Surface modification of silica nanoparticles to reduce aggregation and nonspecific binding. Langmuir. 2006;22:4357–62.
62. Wilhelmand C, Gazeau F. Universal cell labelling with anionic magnetic nanoparticles. Biomaterials. 2008;29:3161–74.
63. Berman S, Walczak P, Bulte JWM. Tracking stem cells using magnetic nanoparticles. Wiley Interdiscipl Rev Nanomedicine Nanobiotechnology. 2011;3:343–55.
64. Ghitescuand L, Fixman A. Surface-charge distribution on the endothelial-cell of liver sinusoids. J Cell Biol. 1984;99:639–47.
65. Drelichand J, Wang YU. Charge heterogeneity of surfaces: mapping and effects on surface forces. Adv Colloid Interface Sci. 2011;165:91–101.
66. Gowrishankarand TR, Weaver JC. An approach to electrical modeling of single and multiple cells. Proc Natl Acad Sci U S A. 2003;100:3203–8.
67. Hoeppener S, Maoz R, Cohen SR, Chi LF, Fuchs H, Sagiv J. Metal nanoparticles, nanowires, and contact electrodes self-assembled on patterned monolayer templates—a bottom-up chemical approach. Adv Mater. 2002;14:1036–41.
68. Smolensky ED, Neary MC, Zhou Y, Berquo TS, Pierre VC. Fe3O4@organic@Au: core-shell nanocomposites with high saturation magnetisation as magnetoplasmonic MRI contrast agents. Chem Commun. 2011;47:2149–51.
69. Laurent S, Forge D, Port M, Roch A, Robic C, Elst LV, Muller RN. Magnetic iron oxide nanoparticles: synthesis, stabilization, vectorization, physicochemical characterizations, and biological applications. Chem Rev. 2008;108:2064–110.